activity, although the former is independent of the latter[25]. To determine whether ILEI interferes with this property, we used three catalytically inactive PS1 mutants: D385A-PS1, CTm2-PS1 and TMD2m-PS1. D385A-PS1 has an alanine substitution of the aspartic acid residue (D^{385}) at the active centre and binds with APP-CTFs and ILEI (Supplementary Fig. 5a–c). CTm2-PS1 has alanine substitutions of D^{385} and the sequential three amino acid residues (D^{458}, Q^{459} and L^{460}) in the extracellular/luminal C-terminal tail and lacks the ability to bind ILEI (Supplementary Fig. 5a,b). TMD2m-PS1, the second transmembrane domain (TMD) of which is replaced with the TMD of CD4 (ref. 26), lacks the ability to bind APP-CTFs (Supplementary Fig. 5c). Overexpression of D385A-PS1 or CTm2-PS1 but not TMD2m-PS1 increased APP-CTFs in PS1/PS2-double knockout mouse embryonic fibroblasts[27] (Supplementary Fig. 5d), suggesting that APP-CTFs are stabilized by the binding with PS1. The APP-CTF-destabilizing effect of ILEI was abrogated by overexpression of CTm2-PS1 or TMD2m-PS1 (Fig. 4g), suggesting that both mutants prevented ILEI from destabilizing APP-CTFs in a dominant-negative manner. Exogenous CTm2-PS1 and TMD2m-PS1 are expected to compete with endogenous PS1 for binding to APP-CTFs and ILEI, respectively. Our results thus imply that APP-CTF destabilization by ILEI requires the interaction between ILEI and PS1, and between PS1 and APP-CTFs. APP-CTFs that accumulated with ILEI knockdown were indeed colocalized with PS1 in subcellular fractions of cultured cells (Supplementary Fig. 3a). These results support our hypothesis that ILEI binds to the PS1/γ-secretase complex and interferes with its APP-CTF-stabilizing property to reduce Aβ generation.

Neuronal expression of ILEI. Previous studies showed that ILEI is expressed in the central nervous system as well as in secretory epithelia[22,28]. However, the regional and cellular distribution of ILEI in mammalian brains has not been examined. We confirmed the specificity of rabbit anti-ILEI antibody (Supplementary Fig. 6) and performed immunohistochemical staining for ILEI. ILEI was widely expressed in mouse and human brains, and was prominent in pyramidal neurons in the cerebral cortex and hippocampus. ILEI-immunoreactive structures were detected in perinuclear regions of neuronal cell bodies, whereas glial fibrillary acidic protein-positive astrocytes and Iba1-positive microglia were negative for ILEI (Fig. 5a). Perinuclear ILEI was colocalized with TGN46, Rab5a and Rab7, indicating that ILEI principally resides in the *trans*-Golgi network and the endocytic vesicles where Aβ is reportedly produced[29,30] (Supplementary Fig. 7). Colocalization of ILEI and APP-CTFs was also confirmed (Supplementary Fig. 8).

Recently, transforming growth factor-β (TGF-β) signalling in neuronal cells was reported to lead to decreased levels of APP-CTF and Aβ[31]. On the other hand, TGF-β selectively induces translation of ILEI via phosphorylation of heterogeneous nuclear ribonucleoprotein E1 in mammary gland cells[32]. Thus, we asked whether the inhibitory effect of TGF-β on Aβ production in brain is mediated by ILEI induction. To address this, we first examined ILEI induction and Aβ reduction by TGF-β using organotypic culture of rat forebrain slices. Next, we evaluated TGF-β-induced reduction in Aβ production from forebrain slices pretreated with ILEI-specific siRNA. TGF-β induced ILEI and reduced Aβ secretion, and these effects were almost completely abrogated in the ILEI-knockdown condition (Fig. 5b).

To evaluate the possible involvement of ILEI in AD pathogenesis, we examined the levels of secreted ILEI in autopsy brains of patients with sporadic AD. Soluble fractions from temporal cortex homogenates were subjected to immunoblotting. ILEI expression was normalized to the level of neuron-specific enolase in each sample to compensate for the difference in neuronal density. ILEI was significantly reduced in AD cases compared with age-matched non-neurological disease controls (Fig. 5c, $P=0.000$) and was inversely correlated with levels of Aβ or phosphorylated tau with semi-quantitative immunoblotting (Supplementary Fig. 9a,b). The ILEI level in autopsy brains with non-AD neurological diseases was equivalent to that of non-neurological disease control brains (Fig. 5c, $P=0.459$). Although our result is preliminary due to the limited number of cases examined, the trend is unequivocal. The decrease in ILEI did not seem to be secondary to brain Aβ accumulation, because ILEI is unaltered in the brains of aged APP-overexpressing mice[33] (Supplementary Fig. 9c).

ILEI ameliorates the phenotypes of AD model mice. To analyse the consequences of ILEI overexpression in mammalian brains, we developed Tg mice in which the mouse prion promoter was used to drive expression of a human ILEI cDNA transgene predominantly in the brain[34]. Heterozygous Tg mice exhibited normal development and fertility with no gross morphological defects. Similar to wild-type mice, ILEI expression was restricted to neuronal cells in the brains of Tg mice (Fig. 6a). Immunoblotting of brain homogenates indicated a three-fold increase in ILEI protein levels and no alteration in Notch intracellular domain levels in the Tg mice compared with non-Tg littermates (Fig. 6b). These findings suggest that the ILEI-Tg mice

Figure 4 | Secreted ILEI interacts with the PS1/γ-secretase complex and interferes with its APP-CTF-stabilizing property. (**a**) Effects of purified ILEI-VH (pILEI-VH) on Aβ secretion and cellular APP-CTFs. pILEI-VH was added to the culture medium of ILEI-knockdown HEK293 cells at the indicated concentrations (μg ml^{-1}). V5-His tag peptide (VH, 7 μg ml^{-1}) served as a negative control. Secreted Aβ40 was measured with ELISA assay and APP-CTFs were analysed with immunoblotting. The right graph shows the relative intensity of APP-CTFs normalized to β-actin ($n=3$, mean ± s.d.). (**b**) Laser scanning confocal microscopic images of pILEI-VH. pILEI-VH was immunostained with anti-V5 tag antibody (green) 0 or 4 h after its addition to the medium. Nuclei were stained with Hoechst 33342 (blue). Scale bar, 10 μm. (**c**) Co-immunoprecipitation assays for pILEI-VH and PS1. ILEI-knockdown HEK293 cells were lysed 0 or 4 h after addition of pILEI-VH, and the cell lysates were subjected to immunoprecipitation. A blot of the anti-ILEI precipitate was probed with anti-PS1-CTF or anti-V5 antibody. (**d**) ILEI-knockdown effects on APP-CTFs and secreted Aβ40 levels in PS1/PS2-knockdown, PEN-2-knockdown, or DAPT (*N*-[*N*-(3,5-difluorophenacetyl)-L-alanyl]-*S*-phenylglycine *t*-butyl ester; 1 μM)-treated HEK293 cells ($n=3$, mean ± s.d.). (**e**) Co-immunoprecipitation assays for PS1 and APP-CTFs. Cell lysates of native, ILEI-knockdown (k/d) and ILEI-overexpressing (oe) HEK293 cells were immunoprecipitated with anti-PS1 antibody (PS1-IP). (**f**) Co-immunoprecipitation assays for PS1 and ILEI. Cell lysates of native and Swedish APP-overexpressing (Sw-APP) HEK293 cells were immunoprecipitated with anti-PS1 antibody (PS1-IP). (**g**) Effects of PS1 mutants on ILEI function. Mock, D385A-PS1, CTm2-PS1 or TMD2m-PS1 was transfected into native, ILEI-knockdown (k/d) and ILEI-overexpressing (oe) HEK293 cells (the same cell lines as in **e**). The same amount of protein from cell membrane lysates was subjected to immunoblotting for APP-CTFs. α: APP-CTFα, β: APP-CTFβ. The graph shows the relative intensity of APP-CTFs normalized to native HEK293 cells transfected with the same plasmid ($n=3$, mean ± s.d.). For data from **a**, **d** and **g**, two-tailed Student's *t*-test was used to analyse statistical significance. $^*P<0.05$, $^{**}P<0.01$ and NS, not significant, versus control (**a**,**d**) or native (**g**).

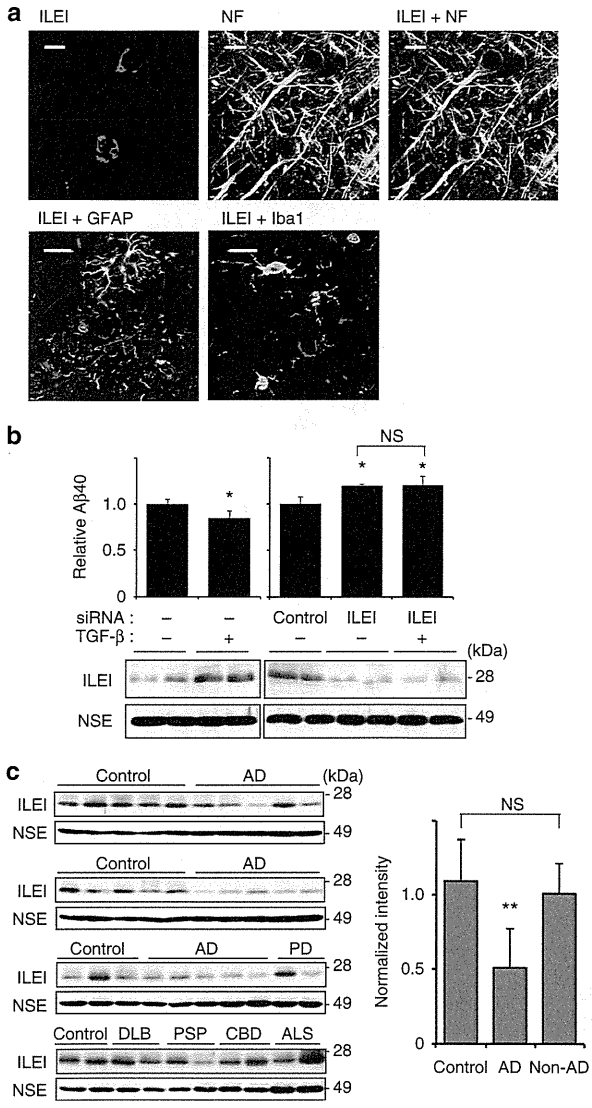

Figure 5 | Neuronal expression of ILEI is induced by TGF-β and reduced in AD brains. (**a**) Double immunostaining for ILEI and cell type-specific markers in mouse brain sections. Neurofilament (NF), glial fibrillary acidic protein (GFAP) and Iba-I are marker proteins for neurons, astrocytes and microglia, respectively. Scale bars, 10 μm. (**b**) Effects of TGF-β treatment on cultured rat brain slices pretreated with non-targeting control or ILEI-specific siRNA. Forebrain slices containing the hippocampus and cerebral cortex were prepared from three Wistar rats (3-week-old, female). The relative levels of Aβ40 ($n=3$, mean ± s.d.) and immunoblotting for ILEI are shown. Neuron-specific enolase (NSE) was used as a loading control. *$P<0.05$ versus vehicle or control, and NS, not significant by Student's *t*-test. Aβ40 concentrations were as follows: control for TGF-β, 743.68 ± 39.32; TGF-β, 631.23 ± 54.36; control for ILEI-knockdown, 751.77 ± 60.23; ILEI-knockdown, 901.28 ± 12.61; ILEI-knockdown/TGF-β, 902.28 ± 72.57 pmol per g protein ($n=3$, mean ± s.d.). (**c**) Immunoblots for ILEI in Tris-buffered saline-extracted fractions from temporal cortices of AD patients ($n=15$, 82.0 ± 4.5 years old, post-mortem interval 7.0 ± 3.5 h), age-matched controls without neurological disease ($n=15$, 80.1 ± 1.7 years old, post-mortem interval 8.0 ± 5.4 h) and non-AD neurological disease controls ($n=10$, 79.6 ± 3.7 years old, post-mortem interval 9.3 ± 5.9 h). Non-AD disease controls were Parkinson's disease (PD), dementia with Lewy bodies (DLB), progressive supranuclear palsy (PSP), corticobasal degeneration (CBD) or amyotrophic lateral sclerosis (ALS). The graph shows the relative intensity of ILEI normalized to NSE (mean ± s.d.). **$P<0.01$ versus control or non-AD control and NS, not significant by Student's *t*-test.

represent an appropriate model for ILEI overexpression without obvious ectopic expression. Immunoblotting revealed a 30% decrease in APP-CTFα and APP-CTFβ levels in the brains of Tg mice compared with controls (Fig. 6c), and the endogenous levels of Aβ40 and Aβ42 in Tris-buffered saline-soluble and -insoluble fractions of brain homogenates were significantly reduced in ILEI-Tg mice compared with non-Tg littermate controls (Fig. 6d). Thus, overexpression of ILEI suppresses APP-CTF accumulation and Aβ generation *in vivo* while sparing Notch processing.

To determine whether ILEI overexpression affects disease progression, we bred ILEI-Tg mice with Swedish mutant APP-overexpressing mice (APP-Tg, Tg2576), which show impaired learning and memory and brain Aβ deposition by 9–10 months of age[33]. APP/ILEI-double Tg mice appeared healthy and had a survival curve comparable with APP-Tg mice. We used a Y-maze test to assess hippocampus-dependent spatial working memory, which declines with age in APP-Tg mice[33]. At 11–13 months of age, but not at 6 months of age, APP-Tg mice showed poor performance ($n=12$, $P=0.0000$), but APP/ILEI-Tg mice showed similar performance ($n=11$, $P=0.3692$) compared with non-Tg littermate (Fig. 7a). We found no significant difference in locomotor activity or motivation to explore the maze (the total number of arm entries was 28.6 ± 3.75 in APP-Tg mice and 25.2 ± 4.08 in APP/ILEI-Tg mice; $P=0.5478$).

We next quantified the Aβ plaque load using brain sections immunohistochemically stained for Aβ. At 12 months of age, the plaque number and the area occupied by plaques in the cerebral cortex and hippocampus were clearly reduced in APP/ILEI-Tg mice compared with APP-Tg littermates (Fig. 7b–d). Moreover, quantitative analysis with Aβ enzyme-linked immunosorbent assay (ELISA) using brains of the same set of mice confirmed that the levels of Aβ40 and Aβ42 in soluble and insoluble fractions were significantly lower in APP/ILEI-Tg mice than in APP-Tg littermates (Fig. 7e,f). These results support the conclusion that ILEI efficiently reduces Aβ accumulation and ameliorates the memory deficit caused by Aβ overload in the brain.

Discussion

Our study shows that Aβ generation can be attenuated by overexpression or administration of ILEI. ILEI regulated Aβ generation by altering the stability of APP-CTFs by extracellular or luminal binding to the PS1/γ-secretase complex. ILEI exhibited functional selectivity for APP and did not affect Notch derivatives. Neuronal expression of ILEI was enhanced by TGF-β signalling in mammalian brain. The levels of secreted ILEI were reduced in autopsy brains of patients with sporadic AD. Tg overexpression of ILEI successfully ameliorated brain Aβ burden and memory deficits in AD model mice.

Based on a recent structural study showing that ILEI and pancreatic-derived factor (PANDER, also known as FAM3B) adopt a globular ββα fold that is distinct from the conformation of classical cytokines, the FAM3 superfamily members may represent a novel class of signalling molecules[35]. Earlier works have revealed that ILEI acts downstream of TGF-β to induce epithelial-to-mesenchymal transition of epithelial cells, whereas PANDER, which is cosecreted with insulin from pancreatic islet cells, is involved in regulation of insulin secretion and glycemic levels[28,36,37]. Expression of the ILEI transcript in human brain has been described[22]. However, the function of ILEI in the nervous system remains largely unknown, except for its possible role in development of the *Xenopus* retina[38]. Our results suggest that ILEI is induced by TGF-β also in mammalian brain. Multiple lines of evidence link TGF-β signalling to brain Aβ accumulation and development of AD[39]. Thus, the specific genotype +10 C/C of the TGF-β1 gene, which affects the expression level of TGF-β1,

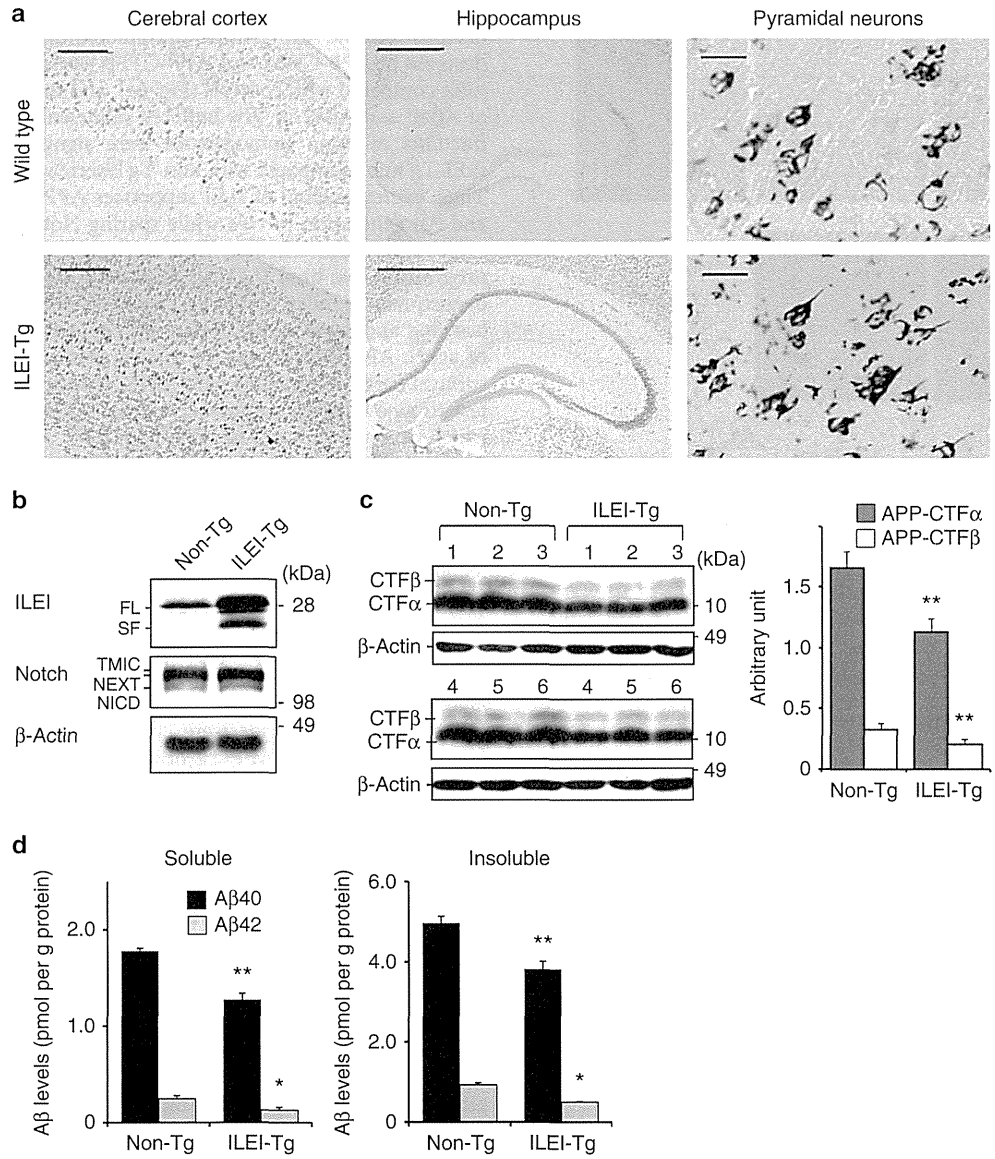

Figure 6 | The Aβ level is reduced in brains of ILEI-Tg mice. (**a**) Immunostaining shows ILEI expression in neurons of the cerebral cortex and hippocampus of wild-type and ILEI-Tg mouse brains (8 months old). Scale bars, 200 μm (left), 500 μm (centre), 20 μm (right). (**b**) Immunoblots for ILEI and Notch in brains of ILEI-Tg mice and non-Tg littermates (6 months old). β-Actin was used as a loading control. FL, full-length; SF, secreted form. (**c**) Immunoblots for APP-CTFs in brains of ILEI-Tg mice and non-Tg littermates (6–8 months old, $n=6$ per genotype). The graph shows the relative intensity of APP-CTFs normalized to β-actin ($n=6$, mean ± s.d.). $^{**}P<0.01$ versus non-Tg mice by Student's *t*-test. (**d**) Brain Aβ levels in non-Tg and ILEI-Tg mice (10 months old, $n=6$ per genotype). Aβ40 (black bars) and Aβ42 (grey bars) in Tris-buffered saline-soluble and -insoluble fractions of brain homogenates were measured using ELISA assays ($n=6$, mean ± s.d.). $^{*}P<0.05$ and $^{**}P<0.01$ versus non-Tg by Student's *t*-test.

is associated with an increased risk of AD[40], and the neuronal expression of TGF-β type II receptors is reduced in AD brains from the early stage of disease development[31]. In addition, recent proteomic analysis of cerebrospinal fluid revealed significantly decreased ILEI levels in patients with idiopathic temporal lobe epilepsy[41], in whom the age-related incidence of Aβ plaques in temporal cortex is significantly higher compared with age-matched controls[42]. The ILEI level in cerebrospinal fluid may also be a biomarker for AD[43]. These reports indirectly support our conclusion, indicating the functional relevance of ILEI to Aβ generation *in vivo* and the pathogenesis of AD.

A previous study using cultured neurons derived from APP-CTFβ-Tg mice indicated that 30% of APP-CTFβ is converted to Aβ[44]. APP-CTFs are also degraded through alternative pathways, including proteasomal, lysosomal and autophagosomal-lysosomal pathways[44–47]. In cultured neuronal cells, proteasome inhibition increases Aβ generation by augmenting the amount of APP-CTFβ[44,45]. Hence, ILEI knockdown may increase Aβ generation by inhibiting APP-CTFβ degradation through pathways that do not lead to Aβ production. Alteration of APP-CTF stability by ILEI required cellular expression of the γ-secretase complex, regardless of whether the complex was enzymatically active or inactive. A large pool of the PS1/γ-secretase complexes remains catalytically inactive in the cell[48]. Even active γ-secretase complexes stably bind to APP-CTFs on substrate-docking sites, which are spatially separated from the catalytic centre[21,49].

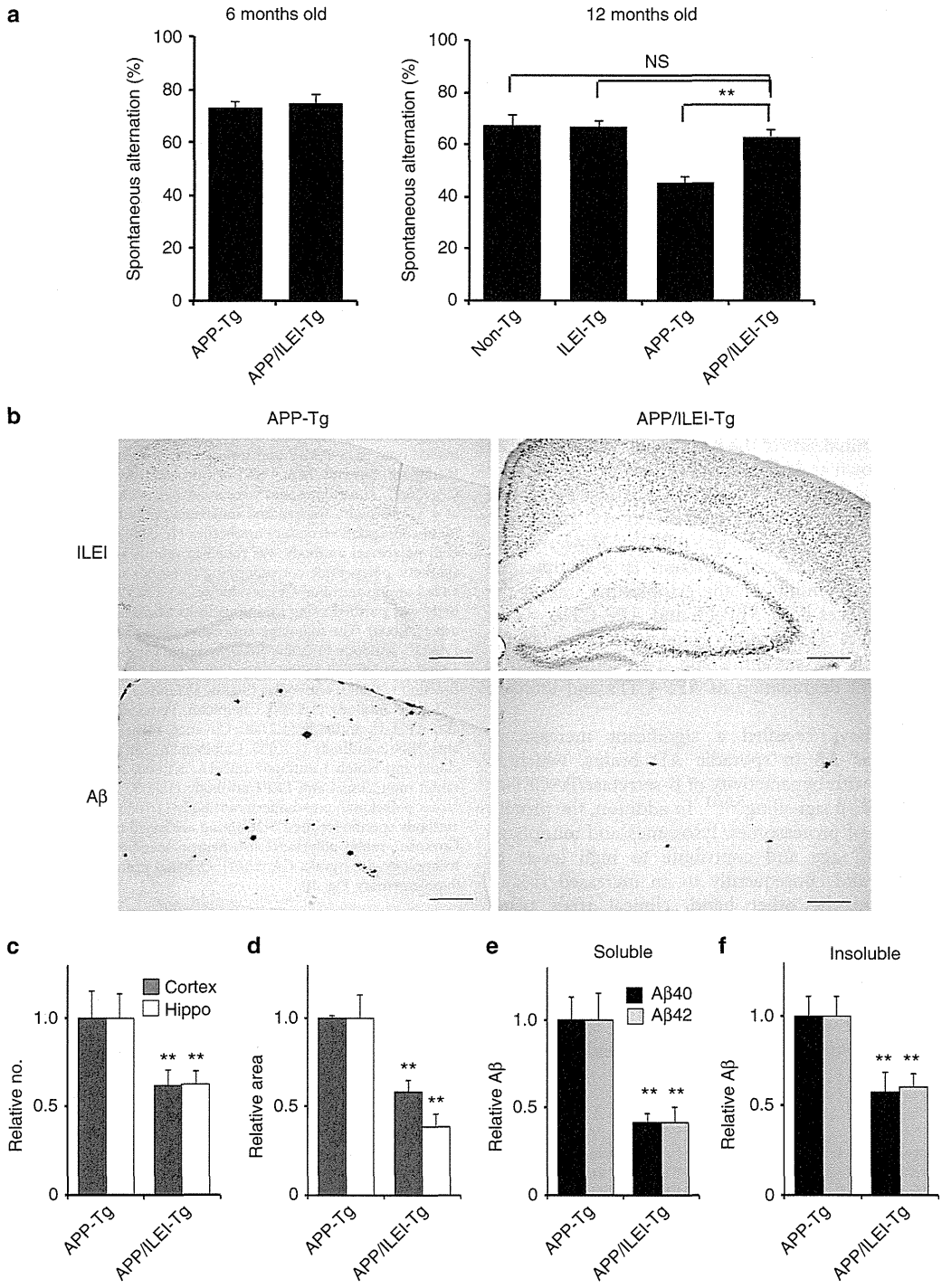

Figure 7 | ILEI overexpression ameliorates the memory deficit and reduces brain Aβ burden in APP-Tg mice. (**a**) Spontaneous alternation in the Y-maze test. APP-Tg (3 females at 6 months age, 6 males and 6 females at 12 months age), ILEI-Tg (5 males and 4 females at 12 months age), APP/ILEI-Tg (3 females at 6 months age, 5 males and 6 females at 12 months age) and non-Tg (5 males and 4 females at 12 months age) littermate mice were used. Data are expressed as percentage (mean ± s.e.m.). $^{**}P<0.01$, NS, not significant by Student's *t*-test. (**b**) Immunostaining images with anti-ILEI antibody (top) and anti-Aβ antibody (bottom) using serial brain sections from 12-month-old APP-Tg (left) and APP/ILEI-Tg (right) mice. Scale bars, 200 μm. (**c**–**f**) Aβ burden in brains of APP-Tg and APP/ILEI-Tg mice (12 months old, $n=6$ per genotype). The plaque number (**c**) and the area occupied by plaques (**d**) in Aβ-immunostained sections of prefrontal cortex (grey bars) and hippocampus (white bars) (mean ± s.e.m.). The relative levels of Aβ40 (black bars) and Aβ42 (grey bars) in soluble (**e**) and insoluble (**f**) fractions (mean ± s.e.m.). $^{**}P<0.01$ versus the APP-Tg by Student's *t*-test. Aβ concentrations were as follows: soluble Aβ40 of APP-Tg, 19.79 ± 2.66; soluble Aβ42 of APP-Tg, 4.69 ± 0.72; insoluble Aβ40 of APP-Tg, 1362.56 ± 152.88; insoluble Aβ42 of APP-Tg, 517.80 ± 57.82; soluble Aβ40 of APP/ILEI-Tg, 8.14 ± 1.21; soluble Aβ42 of APP/ILEI-Tg, 1.95 ± 0.42; insoluble Aβ40 of APP/ILEI-Tg, 788.68 ± 142.23; insoluble Aβ42 of APP/ILEI-Tg, 312.92 ± 38.80 pmol per g protein (mean ± s.e.m.).

Enhanced expression of PS1 in cultured insect and mammalian cells increases the accumulated level of APP-CTFβ by extending its half-life independent of γ-secretase activity[25]. Thus, the PS1/γ-secretase complex also functions as a chaperone that protects APP-CTFs from nonspecific degradation. Chaperone properties of the γ-secretase complex have been described only for APP but not for other substrates. Our results indicate that ILEI inhibits this stabilizing ability by directly binding to PS1-CTF without inhibiting γ-secretase activity, resulting in decreased accumulation of APP-CTFs and diminished generation of Aβ. This possibility is supported by the finding that ILEI is localized in the *trans*-Golgi network and the endocytic vesicles where PS1:CTFβ complexes are located and Aβ is produced[29,30].

Several proteins regulate the stability of APP by directly binding or phosphorylating its cytoplasmic domain[50]. In contrast, ILEI selectively accelerated γ-secretase-independent degradation of APP-CTFs through a novel mechanism in which ILEI interacted with the PS1/γ-secretase complex but not APP on the extracellular or luminal side of the membrane. Modifier of cell adhesion, which is known as dedicator of cytokinesis 3, a member of the dedicator of cytokinesis family of guanine nucleotide exchange factors, binds presenilins and selectively accelerates proteasome-mediated degradation of APP[51]. However, in contrast to ILEI, modifier of cell adhesion is a cytoplasmic protein that binds to presenilins on the cytoplasmic side of the membrane and destabilizes both APP-FL and APP-CTFs via an unknown mechanism[52]. Conversely, platelet-activating factor acetylhydrolase, isoform 1b, subunit 2 and sphingolipids inhibit γ-secretase-independent degradation of APP-CTFs and increase Aβ production[53,54].

Previous studies have revealed a significant increase in APP-CTFβ as well as Aβ in sporadic AD brains, which is sometimes associated with hyperactivity of β-secretase/BACE1 or downregulation of TGF-β signalling[5,6,31]. In addition, the protein degradation activities of proteasomes, lysosomes and autophagy gradually decline with age and contribute to high levels of APP-CTFβ and Aβ, and consequently to an increased risk of sporadic AD[7,8,45]. On the other hand, clinical trials using non-selective inhibitors of γ-secretase activity were discontinued due to adverse effects that were probably caused by Notch inhibition and APP-CTF accumulation[11–13,55]. Thus, ILEI may be a plausible target for the development of disease-modifying therapies for AD, because ILEI may alter disease progression without perturbing Notch signalling and increasing APP-CTFβ.

Methods

Plasmids. For construction of srPEN-2 (ref. 24), three silent nucleotide substitutions were introduced into human PEN-2 cDNA by PCR-based site-directed mutagenesis using the primer: 5′-GAACAGAGCCAAATCAAAGGTTACGTAT GGCGCTCAGCTGTGGGCTTCCTCTTC-3′. The pcDNA3-TAP plasmid containing DNA for the TAP tag, which consists of two immunoglobulin-binding domains of protein A from *Staphylococcus aureus*, a cleavage site for the tobacco etch virus (TEV) protease and the calmodulin-binding polypeptide, was obtained from Dr K. Oshikawa (Kyushu Universiy, Fukuoka, Japan). To generate pTAP-srPEN-2, the TAP tag fragment was fused in-frame to the 5′-end of srPEN-2 cDNA in pcDNA4 (Invitrogen, Carlsbad, CA, USA). A cDNA encoding ILEI with or without the stop codon was amplified from a human brain cDNA library (Clontech, San Diego, CA, USA) using PCR and was then ligated into pcDNA6/V5-His (Invitrogen). To construct the ILEI knockdown vector, the oligonucleotide 5′-GGAGAAGUAUUAGACACU-3′ was ligated into pSUP (Oligoengine, Seattle, WA, USA). To prepare an expression plasmid for siRNA-resistant ILEI, five neutral mutations were introduced into ILEI cDNA by PCR-based site-directed mutagenesis using the primer: 5′-GAAAAACAGGAGAGGTTCTGGATACTAA ATATTTTG-3′. The expression plasmids for PS1 mutants were constructed by PCR-based mutagenesis using the expression plasmid for wild-type human PS1 (ref. 56) as template. The sequences of all constructs were confirmed by sequencing. NotchΔE[57] and HES-Y[58] are gifts from Drs Raphael Kopan (Washington University, St Louis, MO, USA) and Masayasu Okochi (Osaka University, Osaka, Japan), respectively.

Identification of ILEI. To generate the HEK-TAP-PEN-2 and HEK-TAP empty cell lines, we transfected HEK293 cells (CRL-1573, ATCC) stably expressing PEN-2-specific siRNA with pTAP-srPEN-2 or pTAP-empty. HEK-TAP-PEN-2 or HEK-TAP-empty cells were homogenized in buffer A (20 mM Tris (pH 7.5), 150 mM NaCl, 0.5 mM EDTA) containing a protease inhibitor cocktail (Roche Diagnostics, Mannheim, Germany). The postnuclear supernatants were centrifuged at 100,000 *g* for 1 h to collect the microsome membrane pellets. The pellet was solubilized in buffer A containing 1% CHAPSO and then mixed with IgG-sepharose beads followed by incubation at 4 °C for 2 h. The mixture was washed with buffer A containing 0.5% CHAPSO. The beads were incubated with 10 U of TEV protease in TEV buffer (10 mM Tris (pH 8.0), 150 mM NaCl, 0.5 mM EDTA, 0.5% CHAPSO) at 4 °C for 12 h. After adjustment of the calcium concentration to 200 μM, the supernatant was mixed with calmodulin resin in three volumes of buffer B (10 mM Tris (pH 8.0), 150 mM NaCl, 1 mM Mg acetate, 1 mM imidazol, 2 mM $CaCl_2$, 0.5% CHAPSO) and then incubated for 5 h at 4 °C. The proteins were eluted with SDS sample buffer and subjected to SDS–PAGE. The gel was stained with silver or SYPRO Ruby (Molecular Probes, Eugene, OR, USA). Bands were excised from the gel, and proteins in each gel piece that contained a specific band or a group of specific bands were digested with trypsin and subjected to liquid chromatography-tandem mass spectrometry followed by a search of the Mascot database.

Immunoblotting analysis. The same amount of protein from cell lysates was loaded onto SDS–PAGE and transferred to a polyvinylidene fluoride membrane (Millipore, Billerica, MA, USA) or nitrocellurose membrane (BioRad, Hercules, CA, USA). The membranes were incubated with the following primary antibodies at 4 °C overnight, washed and incubated with corresponding horseradish peroxidase-conjugated secondary antibodies (1:3,500, Invitrogen) for 1 h. Anti-human ILEI polyclonal antibody was raised in rabbits against a thyroglobulin-conjugated synthetic polypeptide corresponding to amino acid residues 126 to 143 with an added amino-terminal Cys residue (C + GGDVAPFIEFLKAIQDGT). This antibody was purified using immunoaffinity chromatography with immobilized antigen (1:4,000). The following antibodies were also used: goat polyclonal anti-FAM3C antibody (1:2,000, R&D Systems, Minneapolis, MN, USA); rabbit polyclonal anti-NCT (1:5,000), anti-APP-CTF (1:10,000) and mouse monoclonal anti-β-actin (1:10,000) antibodies (Sigma, St Louis, MO, USA); mouse monoclonal anti-PS1 loop antibody (1:3,500, Chemicon, Temecula, CA, USA); rabbit polyclonal anti-APH-1L antibody (1:2,000, Covance, Princeton, NJ, USA); rabbit polyclonal anti-PEN-2 antibody (1:2,000, Calbiochem, San Diego, CA, USA); mouse monoclonal anti-Notch-1 antibody (mN1A, 1:1,000, AbD Serotec, Kidlington, UK); rabbit monoclonal anti-LRP1 antibody (1:5,000, Abcam, Cambridge, MA, USA); rabbit polyclonal anti-cadherin antibody (1:10,000, Sigma); mouse monoclonal antibody specific for the 17–26 amino acid residues of the human Aβ (4G8, 1:1,000, Covance); rabbit polyclonal anti-neuron-specific enolase (1:10,000, Assay Biotechnology, Sunnyvale, CA, USA). Original immunoblots can be found in Supplementary Fig. 10.

Co-immunoprecipitation and chemical crosslinking. Cultured cells were lysed in a lysis buffer containing 1% CHAPSO. After pre-clearing with protein G-Sepharose 4 fast flow (GE Healthcare, Tokyo, Japan) for 1 h, postnuclear supernatants were incubated with the appropriate antibody. The immunoprecipitates were recovered by overnight incubation with protein G-Sepharose and were analysed with immunoblotting. To eliminate IgG light-chain bands on immunoblots, signals were detected with horseradish peroxidase-conjugated bio-nanocapsules incorporating IgG Fc-binding *Z* domains derived from *S. aureus* protein A[59] (Beacle, Kyoto, Japan) instead of the secondary antibody. For crosslinking, HEK293 cells were treated with 2 mM dithiobis succinimidyl propionate (Thermo Fisher Scientific, Kanagawa, Japan) for 2 h on ice. The reaction was stopped by adding Tris–HCl (pH 7.5, final 20 mM). After incubating on ice for 15 min, the cells were lysed with a lysis buffer containing 1% Nonidet P-40. Under this condition, non-crosslinked components of the γ-secretase complex were reduced by >80% on immunoblotting. After centrifugation at 12,000*g*, the supernatant was subjected to co-immunoprecipitation.

RNA interference. The following siRNA duplexes were purchased from Dharmacon (Lafayette, CO, USA): siGENOME SMART pool M-020514 for ILEI and D001210 for a non-targeting control. The M-020514 pool consisted of the four duplexes targeting the following sequences; F1: 5′-GAACAGCACAUAAAGAA CA-3′; F2: 5′-GGAGAAGUAUUAGACACUA-3′; F3: 5′-GGAGCACAUCUA UUACUAA-3′; F4: 5′-GAACAAUAAGGAUACAAAC-3′. Cultured cells were transfected with individual or pooled siRNA duplexes using Lipofectamine RNAi MAX (Invitrogen).

Secretase activity assays. For a cell-free γ-secretase assay, cultured cells were homogenized in HEPES buffer (25 mM HEPES (pH 7.0), 150 mM NaCl, 5 mM $MgCl_2$, 5 mM $CaCl_2$, a protease inhibitor cocktail) and the postnuclear supernatants were centrifuged at 100,000 *g* for 1 h. The membrane pellets were lysed in 1% CHAPSO/HEPES buffer. Solubilized γ-secretase was recovered by centrifugation at 100,000 *g* for 30 min, and the concentrations of protein and CHAPSO were adjusted to 0.25 mg ml^{-1} and 0.25%, respectively. The resulting

CHAPSO-solubilized γ-secretase was incubated with a recombinant APP-C99-Flag substrate for 6 h at 37 °C, and the Aβ40 and Aβ42 levels were measured by ELISA (WAKO Pure Chemical Industries, Osaka, Japan). For the NICD reporter assay, HEK293 cells in a 12-well plate were transiently transfected with NotchΔE (125 ng), HES-Y (125 ng) and 1.25 ng of the control *Renilla* luciferase reporter plasmid pRL-TK (Promega, Osaka, Japan). The cells were lysed 24 h after transfection, and firefly and *Renilla* luciferase activities were quantified using a dual luciferase reporter assay system (Promega) and a luminometer AB-2250 (Atto, Tokyo, Japan). β-Secretase activity of cell lysates was measured using a fluorometric reaction based on β-secretase cleavage of a synthetic substrate (R&D Systems).

Organotypic brain culture. Sagittal forebrain slices containing the hippocampus and cerebral cortex (400-μm thick) were prepared from 3-week-old female Wistar rats using a vibratome (Lancer Vibratome Series 1000, Vibratome, St Louis, MO, USA). The slices were cultured on semi-porous membrane inserts in six-well plates (0.4-μm pore diameter, Millipore) in a 37 °C, 5% CO_2, 99% humidity incubator. The slices were maintained in standard medium consisting of DMEM Ham's F12, 2% B27 neuronal supplement (Invitrogen) and antibiotic mixture (5 μg ml^{-1} penicillin, 5 μg ml^{-1} streptomycin and 10 μg ml^{-1} gentamycin). After 48 h, slices were treated with 10 ng ml^{-1} TGF-β1 (PeproTech, Rocky Hill, CT, USA) and rat ILEI-specific or non-targeting siRNA (Dharmacon) in Accell siRNA Delivery medium (Dharmacon) for another 48 h.

Autopsy human brain tissues. Frozen brain tissues from the frontal and temporal cortices of 15 patients with AD, 15 age-matched non-neurological disease control subjects and 10 non-AD neurological disease control subjects were obtained from the Brain Bank for Aging Research, Tokyo Metropolitan Institute of Gerontology (Tokyo, Japan). All the study subjects or their next of kin gave written informed consent for the brain donation, and the Shiga University of Medical Science Review Board approved the study protocol. All patients with AD fulfilled the National Institute of Neurological and Communicative Disorders and Stroke-Alzheimer's Disease and Related Disorders Associations criteria for probable AD.

Mice. The Tg vector pMoPrP-ILEI was constructed by subcloning an *Xho*I–*Xho*I fragment of human ILEI cDNA into the *Xho*I site of the MoPrP vector that contains the mouse prion promoter to achieve neuron-specific expression[34]. Tg mice were generated by injection of linearized pMoPrP-ILEI DNA into fertilized C57BL/6 mouse oocytes using standard techniques. Tg founders were identified using PCR (see below). Five founders from each injection were backcrossed to C57BL/6 mice for one to two generations before protein and morphology analysis, and the two lines with the highest expression levels were retained for further experiments. The genotypes of Tg mice were determined by PCR using the following transgene-specific primer pair; mPrP-s 5′-CTGCTCCATTTTGC GTGACTC-3′ and hFAM3C-as 5′-CTTCCAGGCAGATTTTGGGTC-3′. APP-Tg (Tg2576) mice[33] were obtained from Taconic Farms (Hudson, NY, USA) and were bred by mating male mice with ILEI-Tg females. Female littermates were used in this study unless otherwise stated. All animal experiments were performed in accordance with national guidelines (Ministry of Education, Culture, Sports, Science, and Technology) and approved by the Shiga University of Medical Science Institutional Animal Care and Use Committees.

Measurement of Aβ in mouse brains. The right halves of mouse brains were homogenized using a motor-driven Teflon/glass homogenizer (ten strokes) in four volumes of Tris-buffered saline (20 mM Tris (pH 7.5), 150 mM NaCl, 0.5 mM EDTA) that contained a protease inhibitor cocktail. The homogenates were centrifuged at 100,000 *g* for 20 min on a TLA 100.4 rotor in a TLX ultracentrifuge (Beckman, Palo Alto, CA, USA). The supernatant was used as the soluble fraction. The pellet was lysed by brief sonication in an initial volume of 6 M guanidine hydrochloride in 50 mM Tris (pH 7.5), and then centrifuged at 100,000 *g* for 10 min. The supernatant was diluted at 1:12 and used as the insoluble fraction. The soluble and insoluble fractions were subjected to a DC protein assay (BioRad) and ELISA assays specific for mouse/rat Aβ40 and Aβ42 (IBL, Gunma, Japan) or for human Aβ40 and Aβ42 (WAKO Pure Chemical Industries). For quantification of Aβ plaque load on brain sections immunostained with anti-human Aβ (1:2,000, IBL), the number of and percentage area occupied by cortical and hippocampal plaques were measured on digital pictures with the ImageJ 1.46 program (National Institutes of Health, Bethesda, MD, USA).

Immunohistochemistry. The left halves of mouse brains were fixed in 4% paraformaldehyde in phosphate buffer. After blocking endogenous peroxidase activity, free-floating brain sections were incubated with appropriately diluted primary antibodies in PBS containing 2% BSA and 0.3% Triton-X100 at 4 °C overnight under horizontal agitation. Sections were then incubated with biotinylated secondary antibodies for 1 h. The immunoreactive products were visualized by incubating with 3,3′-diaminobenzidine containing nickel ammonium sulphate as an enhancing reagent. Stained sections were observed using a microscope (Olympus BX50, Tokyo, Japan). For double fluorescent immunostaining, sections were incubated with a mixture of rabbit polyclonal anti-ILEI antibody (1:4,000) and mouse monoclonal antibody against non-phosphorylated neurofilament (1:4,000, Covance), glial fibrillary acidic protein (1:4,000, Dako, Tokyo, Japan) or Iba1 (1:2,000, WAKO Pure Chemical Industries) overnight at 4 °C, then reacted with a mixture of secondary antibodies conjugated with Alexa488 (1:500, green) and Alexa594 (1:500, red) (Molecular Probes). The stained sections were analysed using a confocal laser-scanning microscope system (Digital Eclipse C1si-Ready, Nikon, Tokyo, Japan).

Y-maze test. The Y-maze apparatus consisted of three arms with grey walls (40 cm long, 10 cm wide, 10 cm high). The insides of the arms were identical, providing no intramaze cues. Each mouse was placed in the centre of the symmetrical Y-maze and was allowed to explore the maze freely for 8 min. The number and sequence of arms entered were recorded manually. The total number of arm entries was used to measure locomotor activity and motivation to explore the maze. The percentage of alternation, which was calculated by the proportion of alternations (an arm choice differing from the previous two choices) to the total number of alternation opportunities (total arm entries minus two), was used as a measure of spatial working memory. Experiments were done blind regarding the genotype of the mice.

Statistical analysis. Statistical evaluation was performed using two-tailed unpaired Student's *t*-test unless otherwise stated. Data are presented as means ± s.d. Statistical significance was defined at $^{*}P<0.05$ or $^{**}P<0.01$.

References

1. De Strooper, B., Iwatsubo, T. & Wolfe, M. S. Presenilins and γ-secretase: structure, function, and role in Alzheimer disease. *Cold Spring Harb. Perspect. Med.* **2,** a006304 (2012).
2. Muller, U. C. & Zheng, H. Physiological functions of APP family proteins. *Cold Spring Harb. Perspect. Med.* **2,** a006288 (2012).
3. Ring, S. *et al.* The secreted β-amyloid precursor protein ectodomain APPsα is sufficient to rescue the anatomical, behavioral, and electrophysiological abnormalities of APP-deficient mice. *J. Neurosci.* **27,** 7817–7826 (2007).
4. St George-Hyslop, P. H. & Petit, A. Molecular biology and genetics of Alzheimer's disease. *C. R. Biol.* **328,** 119–130 (2005).
5. Fukumoto, H., Cheung, B. S., Hyman, B. T. & Irizarry, M. C. β-secretase protein and activity are increased in the neocortex in Alzheimer disease. *Arch. Neurol.* **59,** 1381–1389 (2002).
6. Yang, L. B. *et al.* Elevated β-secretase expression and enzymatic activity detected in sporadic Alzheimer disease. *Nat. Med.* **9,** 3–4 (2003).
7. Riederer, B. M., Leuba, G., Vernay, A. & Riederer, I. M. The role of the ubiquitin proteasome system in Alzheimer's disease. *Exp. Biol. Med. (Maywood)* **236,** 268–276 (2011).
8. Nixon, R. A. & Yang, D. S. Autophagy failure in Alzheimer's disease--locating the primary defect. *Neurobiol. Dis.* **43,** 38–45 (2011).
9. Chang, K. A. & Suh, Y. H. Pathophysiological roles of amyloidogenic carboxy-terminal fragments of the β-amyloid precursor protein in Alzheimer's disease. *J. Pharmacol. Sci.* **97,** 461–471 (2005).
10. Bittner, T. *et al.* γ-secretase inhibition reduces spine density *in vivo* via an amyloid precursor protein-dependent pathway. *J. Neurosci.* **29,** 10405–10409 (2009).
11. Wong, G. T. *et al.* Chronic treatment with the γ-secretase inhibitor LY-411,575 inhibits β-amyloid peptide production and alters lymphopoiesis and intestinal cell differentiation. *J. Biol. Chem.* **279,** 12876–12882 (2004).
12. Mitani, Y. *et al.* Differential effects between γ-secretase inhibitors and modulators on cognitive function in amyloid precursor protein-transgenic and nontransgenic mice. *J. Neurosci.* **32,** 2037–2050 (2012).
13. Doody, R. S. *et al.* A phase 3 trial of semagacestat for treatment of Alzheimer's disease. *N. Engl. J. Med.* **369,** 341–350 (2013).
14. De Strooper, B. & Annaert, W. Novel research horizons for presenilins and γ-secretases in cell biology and disease. *Annu. Rev. Cell. Dev. Biol.* **26,** 235–260 (2010).
15. Mitsuishi, Y. *et al.* Human CRB2 inhibits γ-secretase cleavage of amyloid precursor protein by binding to the presenilin complex. *J. Biol. Chem.* **285,** 14920–14931 (2010).
16. Hasegawa, H., Liu, L. & Nishimura, M. Dilysine retrieval signal-containing p24 proteins collaborate in inhibiting γ-cleavage of amyloid precursor protein. *J. Neurochem.* **115,** 771–781 (2010).
17. He, G. *et al.* γ-secretase activating protein is a therapeutic target for Alzheimer's disease. *Nature* **467,** 95–98 (2010).
18. Chen, F. *et al.* TMP21 is a presenilin complex component that modulates γ-secretase but not ε-secretase activity. *Nature* **440,** 1208–1212 (2006).
19. Wakabayashi, T. *et al.* Analysis of the γ-secretase interactome and validation of its association with tetraspanin-enriched microdomains. *Nat. Cell. Biol.* **11,** 1340–1346 (2009).

20. Rigaut, G. *et al.* A generic protein purification method for protein complex characterization and proteome exploration. *Nat. Biotechnol.* **17,** 1030–1032 (1999).
21. Esler, W. P. *et al.* Activity-dependent isolation of the presenilin-γ-secretase complex reveals nicastrin and a γ substrate. *Proc. Natl Acad. Sci. USA* **99,** 2720–2725 (2002).
22. Zhu, Y. *et al.* Cloning, expression, and initial characterization of a novel cytokine-like gene family. *Genomics* **80,** 144–150 (2002).
23. Zhao, G., Liu, Z., Ilagan, M. X. & Kopan, R. γ-secretase composed of PS1/Pen2/Aph1a can cleave Notch and amyloid precursor protein in the absence of nicastrin. *J. Neurosci.* **30,** 1648–1656 (2010).
24. Hasegawa, H. *et al.* Both the sequence and length of the C terminus of PEN-2 are critical for intermolecular interactions and function of presenilin complexes. *J. Biol. Chem.* **279,** 46455–46463 (2004).
25. Pitsi, D. & Octave, J. N. Presenilin 1 stabilizes the C-terminal fragment of the amyloid precursor protein independently of γ-secretase activity. *J. Biol. Chem.* **279,** 25333–25338 (2004).
26. Watanabe, N. *et al.* Functional analysis of the transmembrane domains of presenilin 1: participation of transmembrane domains 2 and 6 in the formation of initial substrate-binding site of γ-secretase. *J. Biol. Chem.* **285,** 19738–19746 (2010).
27. Herreman, A. *et al.* Total inactivation of γ-secretase activity in presenilin-deficient embryonic stem cells. *Nat. Cell Biol.* **2,** 461–462 (2000).
28. Waerner, T. *et al.* ILEI: a cytokine essential for EMT, tumor formation, and late events in metastasis in epithelial cells. *Cancer Cell* **10,** 227–239 (2006).
29. Xia, W. *et al.* Presenilin complexes with the C-terminal fragments of amyloid precursor protein at the sites of amyloid β-protein generation. *Proc. Natl Acad. Sci. USA* **97,** 9299–9304 (2000).
30. Choy, R. W., Cheng, Z. & Schekman, R. Amyloid precursor protein (APP) traffics from the cell surface via endosomes for amyloid β (Aβ) production in the trans-Golgi network. *Proc. Natl Acad. Sci. USA* **109,** E2077–E2082 (2012).
31. Tesseur, I. *et al.* Deficiency in neuronal TGF-β signaling promotes neurodegeneration and Alzheimer's pathology. *J. Clin. Invest.* **116,** 3060–3069 (2006).
32. Chaudhury, A. *et al.* TGF-β-mediated phosphorylation of hnRNP E1 induces EMT via transcript-selective translational induction of Dab2 and ILEI. *Nat. Cell Biol.* **12,** 286–293 (2010).
33. Hsiao, K. *et al.* Correlative memory deficits, Aβ elevation, and amyloid plaques in transgenic mice. *Science* **274,** 99–102 (1996).
34. Borchelt, D. R. *et al.* A vector for expressing foreign genes in the brains and hearts of transgenic mice. *Genet. Anal.* **13,** 159–163 (1996).
35. Johansson, P. *et al.* FAM3B PANDER and FAM3C ILEI represent a distinct class of signaling molecules with a non-cytokine-like fold. *Structure* **21,** 306–313 (2013).
36. Lahsnig, C. *et al.* ILEI requires oncogenic Ras for the epithelial to mesenchymal transition of hepatocytes and liver carcinoma progression. *Oncogene* **28,** 638–650 (2009).
37. Wilson, C. G., Robert-Cooperman, C. E. & Burkhardt, B. R. PANcreatic-DERived factor: novel hormone PANDERing to glucose regulation. *FEBS Lett.* **585,** 2137–2143 (2011).
38. Katahira, T., Nakagiri, S., Terada, K. & Furukawa, T. Secreted factor FAM3C (ILEI) is involved in retinal laminar formation. *Biochem. Biophys. Res. Commun.* **392,** 301–306 (2010).
39. Caraci, F. *et al.* TGF-β1 pathway as a new target for neuroprotection in Alzheimer's disease. *CNS Neurosci. Ther.* **17,** 237–249 (2011).
40. Caraci, F. *et al.* The CC genotype of transforming growth factor-β1 increases the risk of late-onset Alzheimer's disease and is associated with AD-related depression. *Eur. Neuropsychopharmacol.* **22,** 281–289 (2012).
41. Xiao, F. *et al.* Proteomic analysis of cerebrospinal fluid from patients with idiopathic temporal lobe epilepsy. *Brain Res.* **1255,** 180–189 (2009).
42. Mackenzie, I. R. & Miller, L. A. Senile plaques in temporal lobe epilepsy. *Acta. Neuropathol.* **87,** 504–510 (1994).
43. Davies, H., Blennow, K., McGuire, J., Podust, V. & Simonsen, A. Saponin D and FAM3C are biomarkers for Alzheimer's disease. US Patent 7993868 (2011).
44. Nunan, J. *et al.* The C-terminal fragment of the Alzheimer's disease amyloid protein precursor is degraded by a proteasome-dependent mechanism distinct from γ-secretase. *Eur. J. Biochem.* **268,** 5329–5336 (2001).
45. Flood, F. *et al.* Proteasome-mediated effects on amyloid precursor protein processing at the γ-secretase site. *Biochem. J.* **385,** 545–550 (2005).
46. Caporaso, G. L., Gandy, S. E., Buxbaum, J. D. & Greengard, P. Chloroquine inhibits intracellular degradation but not secretion of Alzheimer β/A4 amyloid precursor protein. *Proc. Natl Acad. Sci. USA* **89,** 2252–2256 (1992).
47. Jaeger, P. A. *et al.* Regulation of amyloid precursor protein processing by the Beclin 1 complex. *PLoS ONE* **5,** e11102 (2010).
48. Lai, M. T. *et al.* Presenilin-1 and presenilin-2 exhibit distinct yet overlapping γ-secretase activities. *J. Biol. Chem.* **278,** 22475–22481 (2003).
49. Sato, C., Takagi, S., Tomita, T. & Iwatsubo, T. The C-terminal PAL motif and transmembrane domain 9 of presenilin 1 are involved in the formation of the catalytic pore of the γ-secretase. *J. Neurosci.* **28,** 6264–6271 (2008).
50. Suzuki, T. & Nakaya, T. Regulation of amyloid β-protein precursor by phosphorylation and protein interactions. *J. Biol. Chem.* **283,** 29633–29637 (2008).
51. Chen, Q., Kimura, H. & Schubert, D. A novel mechanism for the regulation of amyloid precursor protein metabolism. *J. Cell Biol.* **158,** 79–89 (2002).
52. Kashiwa, A. *et al.* Isolation and characterization of novel presenilin binding protein. *J. Neurochem.* **75,** 109–116 (2000).
53. Page, R. M. *et al.* Loss of PAFAH1B2 reduces amyloid-β generation by promoting the degradation of amyloid precursor protein C-terminal fragments. *J. Neurosci.* **32,** 18204–18214 (2012).
54. Tamboli, I. Y. *et al.* Sphingolipid storage affects autophagic metabolism of the amyloid precursor protein and promotes Aβ generation. *J. Neurosci.* **31,** 1837–1849 (2011).
55. Chavez-Gutierrez, L. *et al.* The mechanism of γ-secretase dysfunction in familial Alzheimer disease. *EMBO J.* **31,** 2261–2274 (2012).
56. Nishimura, M. *et al.* Presenilin mutations associated with Alzheimer disease cause defective intracellular trafficking of β-catenin, a component of the presenilin protein complex. *Nat. Med.* **5,** 164–169 (1999).
57. Schroeter, E. H., Kisslinger, J. A. & Kopan, R. Notch-1 signalling requires ligand-induced proteolytic release of intracellular domain. *Nature* **393,** 382–386 (1998).
58. Tagami, S. *et al.* Regulation of Notch signaling by dynamic changes in the precision of S3 cleavage of Notch-1. *Mol. Cell Biol.* **28,** 165–176 (2008).
59. Iijima, M. *et al.* Nanocapsules incorporating IgG Fc-binding domain derived from *Staphylococcus aureus* protein A for displaying IgGs on immunosensor chips. *Biomaterials* **32,** 1455–1464 (2011).
60. Edbauer, D., Willem, M., Lammich, S., Steiner, H. & Haass, C. Insulin-degrading enzyme rapidly removes the β-amyloid precursor protein intracellular domain (AICD). *J. Biol. Chem.* **277,** 13389–13393 (2002).

Acknowledgements

This work was supported in part by Grants-in-Aid for Scientific Research from the Ministry of Education, Culture, Sports, Science, and Technology, Japan (23500445 to M.N. and 23590359 to H.H.), a grant from the A-STEP, Japan Science and Technology Agency (AS231Z00919G to M.N.) and a grant from the Program for the Promotion of Fundamental Studies in Health Sciences of the National Institute of Biomedical Innovation, Japan (05-26 to M.N.).

Author contributions

H.H. and L.L. performed the TAP and cell culture experiments. L.L. contributed to the organotypic culture and immunohistochemistry experiments. L.L., I.T. and M.N. carried out the Tg mouse experiments. S.M. collected autopsy brain samples and performed neuropathological diagnosis. M.N. designed the study, supervised all of the experiments and wrote the manuscript.

Additional information

Supplementary Information accompanies this paper at http://www.nature.com/naturecommunications

Competing financial interests: The authors declare no competing financial interests.

Reprints and permission information is available online at http://npg.nature.com/reprintsandpermissions/

How to cite this article: Hasegawa, H. *et al.* The FAM3 superfamily member ILEI ameliorates Alzheimer's disease-like pathology by destabilizing the penultimate amyloid-β precursor. *Nat. Commun.* 5:3917 doi: 10.1038/ncomms4917 (2014).

Supplementary Figure 1

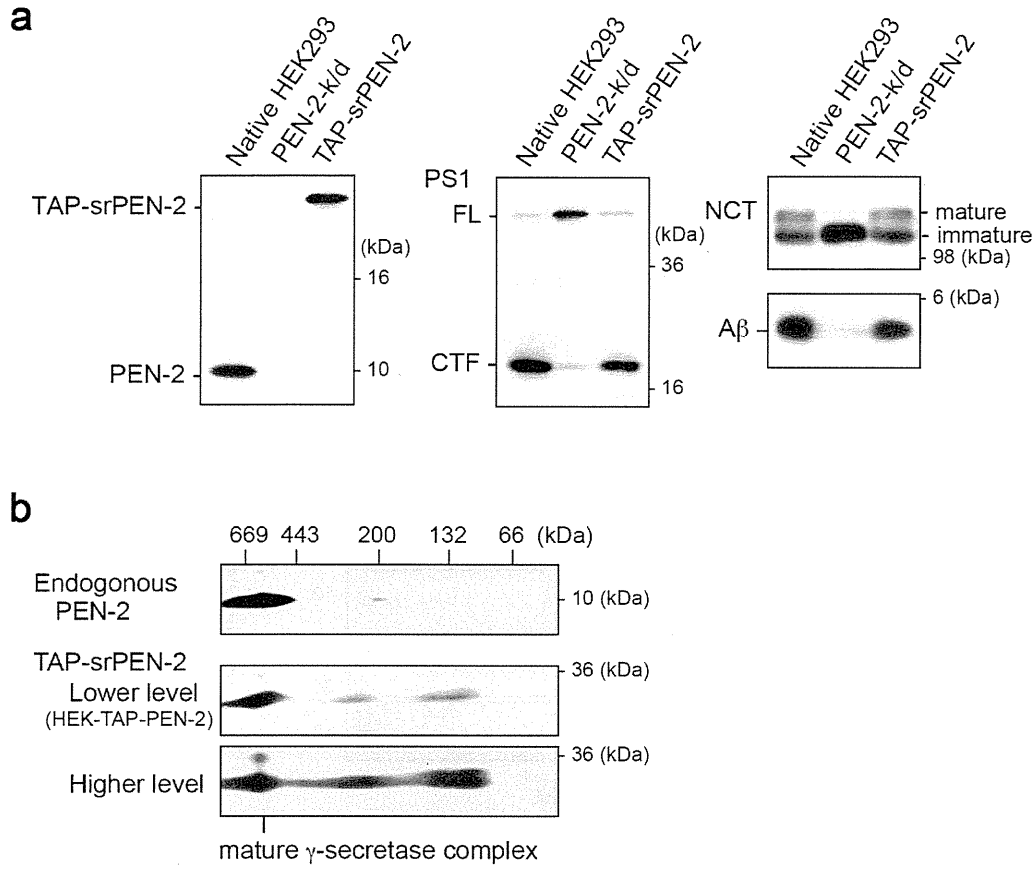

Supplementary Figure 1. Characterization of HEK/TAP-PEN-2 cells

(a) Stable transfection of PEN2-knockdown (k/d) HEK293 cells with TAP-srPEN-2 (left panel) restored proteolysis of PS1 (center panel), glycosylation of NCT (right upper panel), and generation of Aβ (right lower panel). Aβ was immunoprecipitated from the conditioned medium of each cell line and subjected to immunoblotting. **(b)** 2D-BN/SDS-PAGE followed by immunoblotting showed that endogenous PEN-2 was incorporated into the mature γ-secretase complex in native HEK293 cells (upper panel). Most of the transfected TAP-srPEN-2 was incorporated into the mature γ-secretase complex in the HEK-TAP-PEN-2 cell line (middle panel), although a cell line with higher TAP-srPEN-2 expression formed multiple smaller complexes (lower panel). Original immunoblots for (**a**) and (**b**) can be found in Supplementary Fig. 10.

Supplementary Figure 2

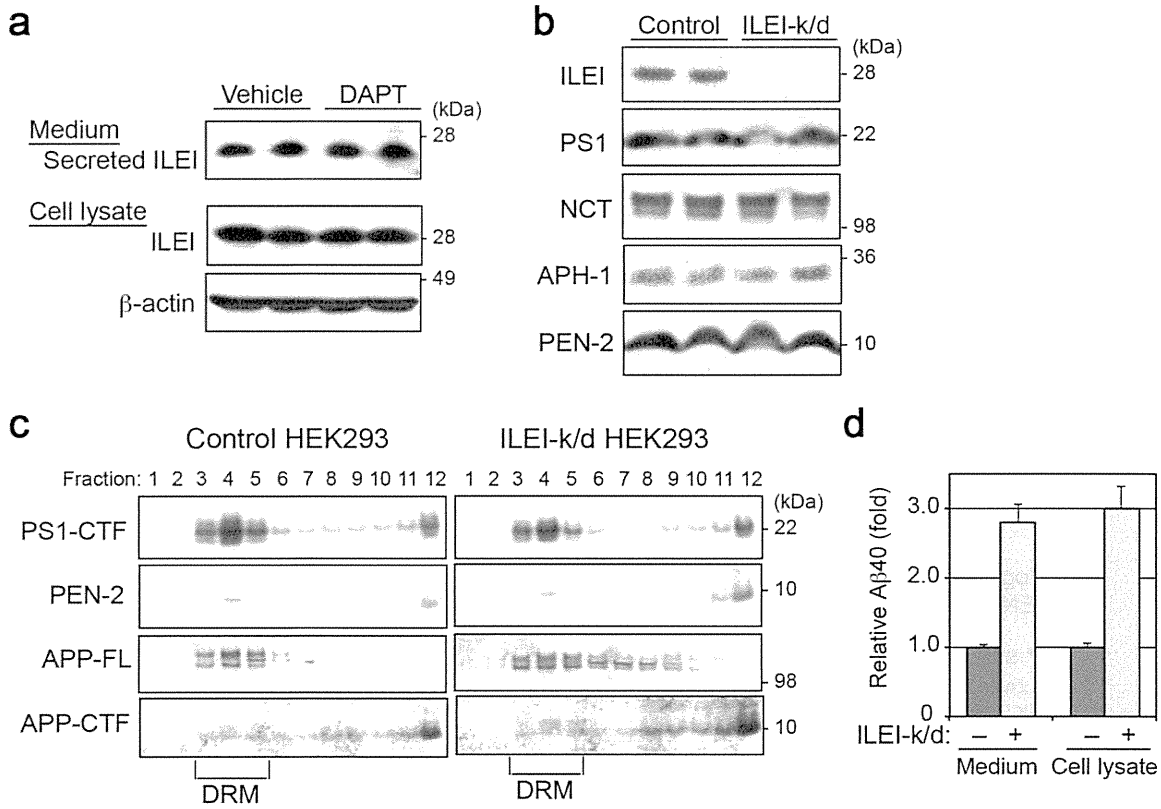

Supplementary Figure 2. ILEI is not a substrate for γ-secretase and does not affect the expression level or the subcellular localization of the γ-secretase complex, or the Aβ secretion process.

(a) DAPT treatment of HEK293 cells did not alter the levels of cellular and secreted ILEI as assessed with immunoblotting. β-actin was used as a loading control. **(b)** ILEI-knockdown (k/d) did not change the expression levels of the indicated γ-secretase components as assessed with immunoblotting. **(c)** ILEI did not detectably affect localization of the γ-secretase complex or APP in detergent-resistant membrane microdomains (DRM). HEK293 cells treated with control or ILEI-specific siRNA were homogenized in MBS buffer (25 mM MES, 150 mM NaCl, pH 6.5) containing 1% Lubrol WX (Lubrol 17A17; Serva) and a protease inhibitor cocktail. The homogenate was centrifuged at 2,000 *g* for 10 min, and the supernatant was adjusted to 40% sucrose in MBS. The sample was transferred to 13-ml ultracentrifuge tubes and overlaid with a 5/10/20/30% discontinuous sucrose gradient in MBS. After centrifugation at 260,000 *g* for 21 h in an SW-41Ti rotor (Beckman Coulter), 1-ml fractions were collected from the top and analyzed with immunoblotting. **(d)** ILEI did not perturb the process of Aβ secretion. ILEI-knockdown increased Aβ levels in both the culture medium and cell lysates of Swedish mutant APP-overexpressing HEK293 cells. Aβ40 concentrations were as follows: control medium, 9.49 ± 0.32 pmol ml^{-1}, ILEI-k/d medium, 26.78 ± 2.86 pmol ml^{-1}; control cell lysate, 13.82 ± 0.88 pmol per g protein; ILEI-k/d cell lysate, 42.55 ± 5.82 pmol per g protein ($n = 3$, mean ± s.d.). $P > 0.05$ by Student's *t*-test. Original immunoblots for (**a-c**) can be found in Supplementary Fig. 10.

Supplementary Figure 3

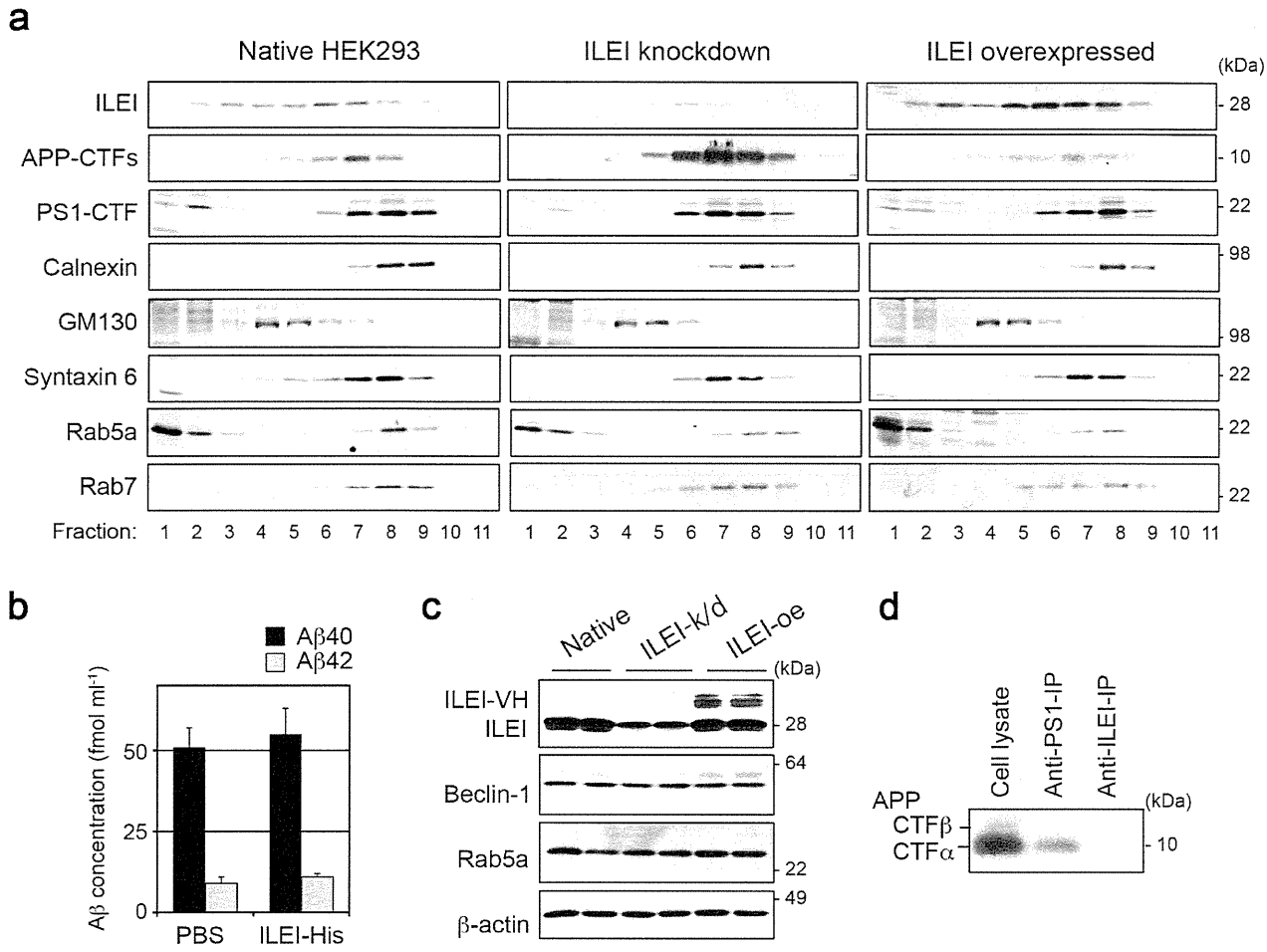

Supplementary Figure 3. ILEI does not alter the general activity of autophagy, lysosomal protein degradation, or subcellular localization of APP-CTFs.

(a) Subcellular localization of ILEI, APP-CTFs, and PS1-CTF in native, ILEI-knockdown and ILEI-overexpressed HEK293 cells. Membrane fractions were isolated from HEK293 cells and applied onto a discontinuous gradient consisting of 1 ml each of 30%, 25%, 20%, 15%, 12.5%, 10%, 7.5%, 5% and 2.5% (v/v) iodixanol. After centrifugation at 126,000 *g* for 1 h, eleven 1.0-ml fractions were collected from the top to the bottom of the gradient and were subjected to immunoblotting with the indicated antibodies. Antibodies against calnexin (1:10,000), GM130 (1:10,000), syntaxin 6 (1:5,000) (BD Transduction Laboratories), Rab5a (1:1,000), and Rab7 (1:500) (Santa Cruz Biotechnology) were used as markers of the endoplasmic reticulum, *cis*-Golgi, *trans*-Golgi, early endosomes, and late endosomes, respectively. **(b)** ILEI did not enhance Aβ degradation in the culture medium. The conditioned medium of ILEI-knockdown cells was incubated with PBS or purified ILEI-VH (5 μg ml^{-1}) at 37 °C for 6 h. Aβ levels were measured using ELISAs ($n = 3$, mean ± s.d.). $P > 0.05$ by Student's *t*-test. **(c)** Lysates of native, ILEI-knockdown (k/d), and ILEI-overexpressing (oe) HEK293 cells were subjected to immunoblotting for ILEI, Beclin-1, and Rab5a. β-actin was used as a loading control. **(d)** Co-immunoprecipitation of ILEI and APP-CTFs. Native HEK293 cell lysates were immunoprecipitated with normal IgG or an antibody against ILEI. The blot was probed with anti-APP-CTF antibody. Anti-PS1 precipitate served as a positive control. Original immunoblots for (**a**), (**c**) and (**d**) can be found in Supplementary Fig. 10.

Supplementary Figure 4

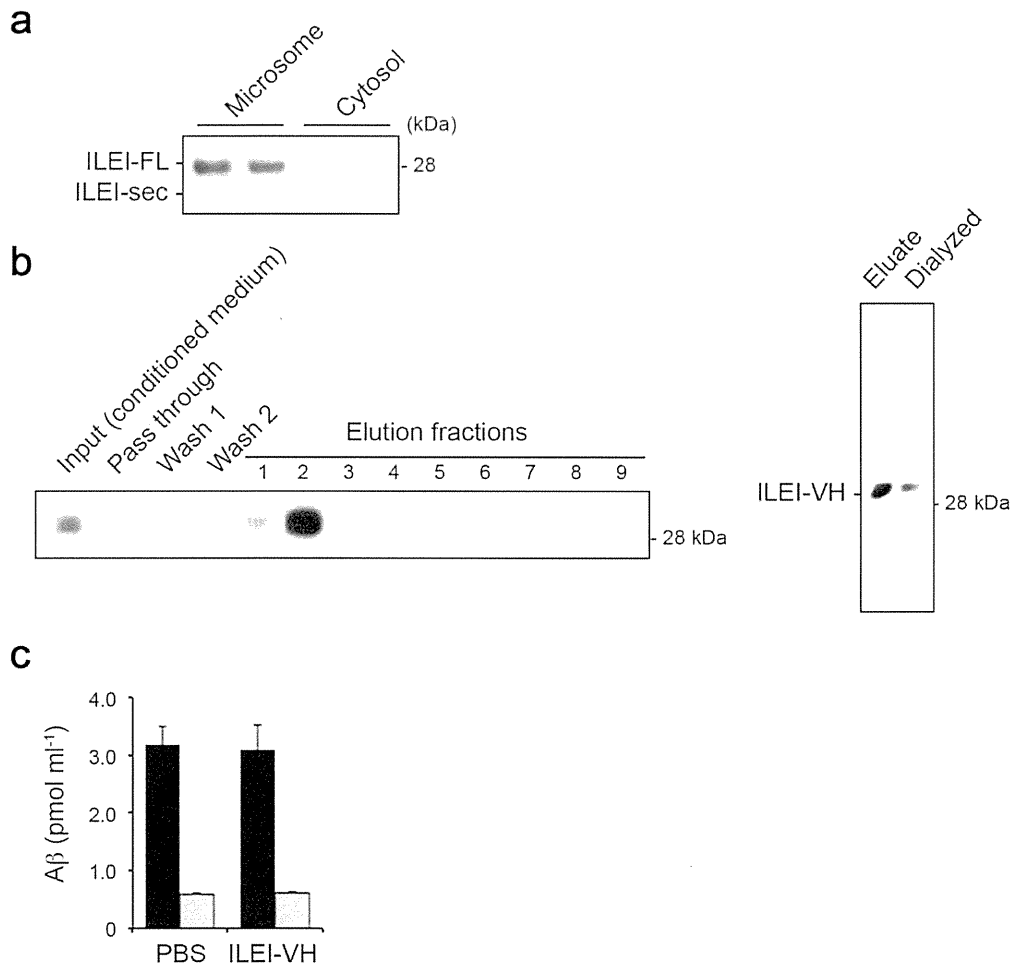

Supplementary Figure 4. Purification of secreted ILEI-VH peptide

(a) Intracellular ILEI was mostly associated with the microsome fraction. The homogenate of HEK293 cells was centrifuged at 1,000 *g*, and the supernatant was further ultracentrifuged at 100,000 *g* for 1 h to yield crude microsome (pellet) and cytosol (supernatant) fractions, which were then assayed with immunoblotting for ILEI. **(b)** Purification of the ILEI-VH peptide. The conditioned medium of HEK293 cells stably overexpressing C-terminally V5-6xHis-tagged ILEI (ILEI-VH) was cleared with brief centrifugation and then incubated with Ni-nitrilotriacetic acid-agarose (Qiagen) for 8 h at 4 °C. After washing twice with PBS, the secreted ILEI-VH was eluted with 200 mM imidazole. The fractions were assayed with immunoblotting for ILEI (left panel). The eluted fraction #2 was dialyzed against PBS. The purity of the ILEI-VH fractions was tested using SDS-PAGE followed by Coomassie Brilliant Blue staining (right panel). **(c)** Purified ILEI-VH did not affect Aβ generation in a cell-free γ-secretase assay. Solubilized γ-secretase complexes prepared from ILEI-knockdown HEK293 cells were incubated with recombinant APP-CTFβ-Flag in the presence or absence of purified ILEI-VH (5 μg ml^{-1}). Aβ40 (black bars) and Aβ42 (grey bars) were measured using ELISAs ($n = 3$, mean ± s.d.). $P > 0.05$ by Student's *t*-test. Original immunoblots for (**a**) and (**b**) can be found in Supplementary Fig. 10.

Supplementary Figure 5

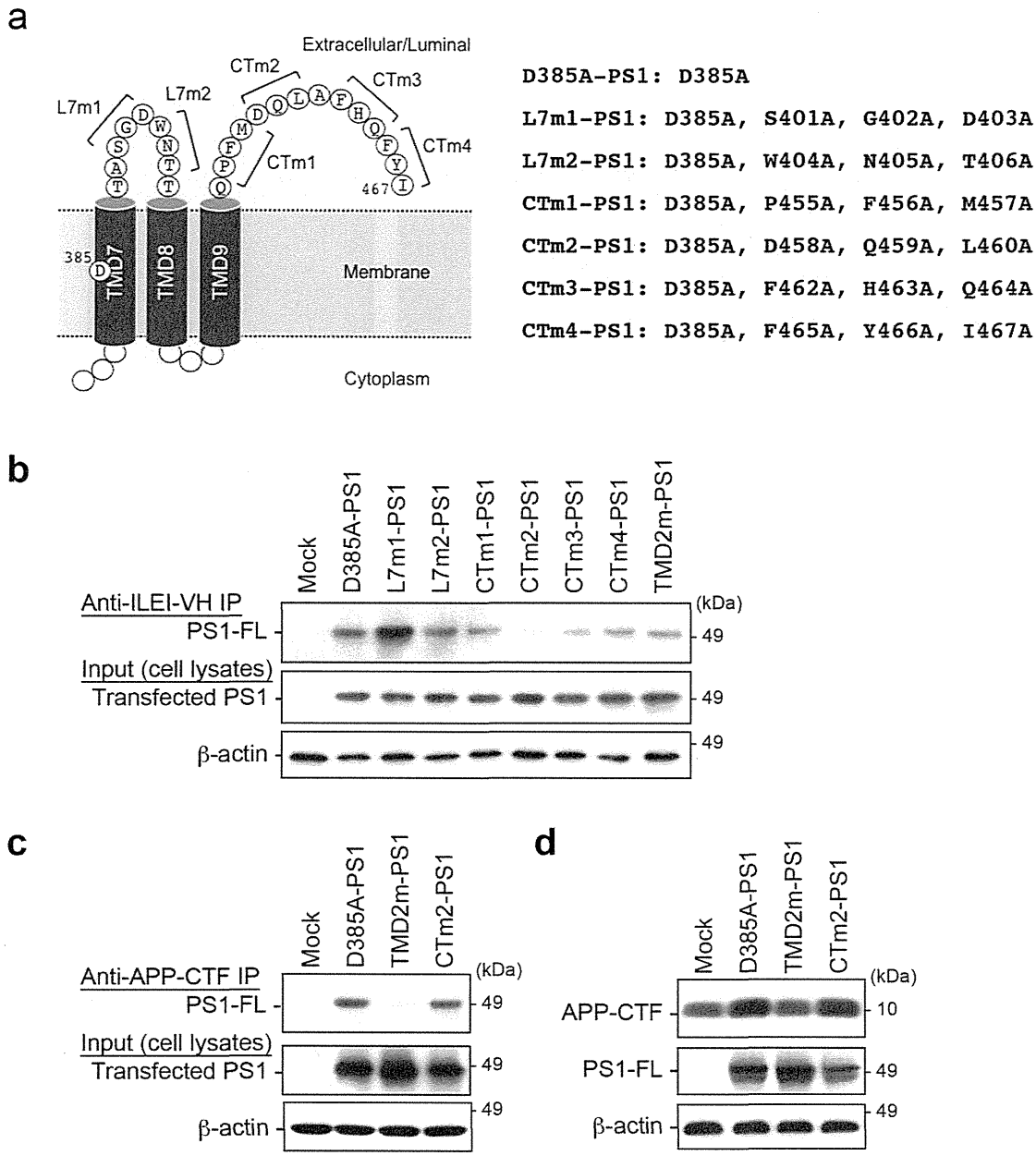

Supplementary Figure 5. Characterization of PS1 mutants

(a) Schematic of PS1 mutants harboring alanine substitutions of the active site aspartate (D^{385}) and three sequential amino acid residues in the extracellular/luminal C-terminal regions. **(b)** Co-immunoprecipitation of mutant PS1 and ILEI. Each PS1 mutant was transiently transfected into HEK293 cells stably expressing ILEI-VH, and IELI-VH was precipitated with anti-V5 antibody. CTm2-PS1 was not co-immunoprecipitated with IELI-VH. **(c)** Co-immunoprecipitation of mutant PS1 and APP. HEK293 cells were transfected with mock, D385A-PS1, TMD2m-PS1, or CTm2-PS1, and then treated with DAPT for 12 h. Anti-APP-CTF precipitates did not contain TMD2m-PS1. **(d)** Mock, D385A-PS1, TMD2m-PS1, or CTm2-PS1 was transfected into PS1/PS2-knockout MEFs. Cell lysates were subjected to immunoblotting for APP-CTFs or PS1. β-actin was used as a loading control. Original immunoblots for (**b-d**) can be found in Supplementary Fig. 10.

Supplementary Figure 6

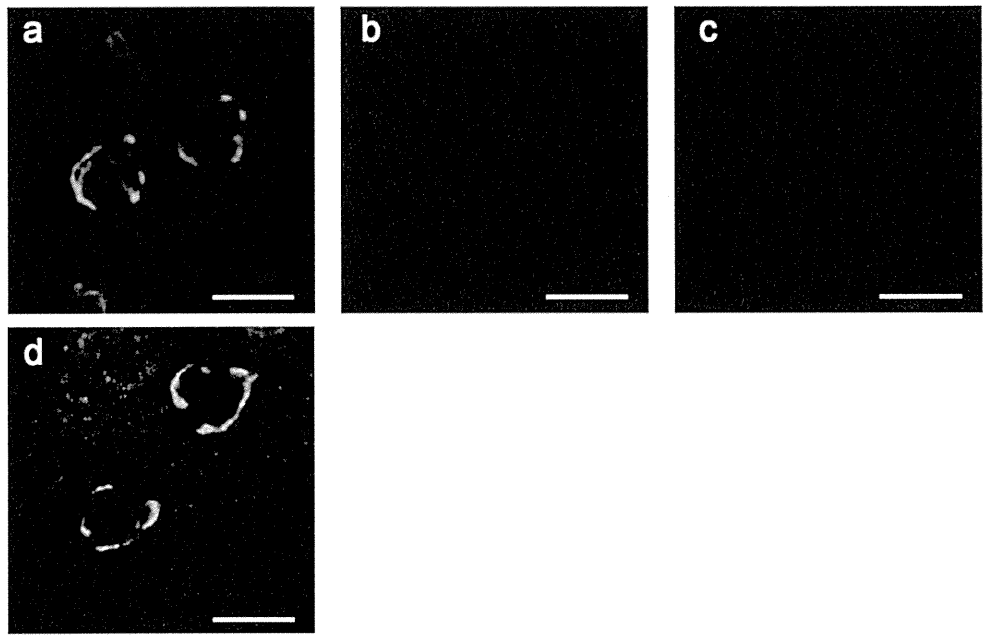

Supplementary Figure 6. Characterization of rabbit polyclonal anti-ILEI antibody

(a) Rabbit polyclonal antibody against a synthetic polypeptide representing the N-terminal sequence of human ILEI immunostained perinuclear vesicular structures in neurons of mouse brain. Incubation with the secondary antibody alone **(b)** or preabsorption of the rabbit antibody with the antigen peptide **(c)** abolished immunostaining. **(d)** Goat polyclonal antibody against human full-length ILEI immunostained similar structures as seen in (a). Scale bars: 10 μm.

Supplementary Figure 7

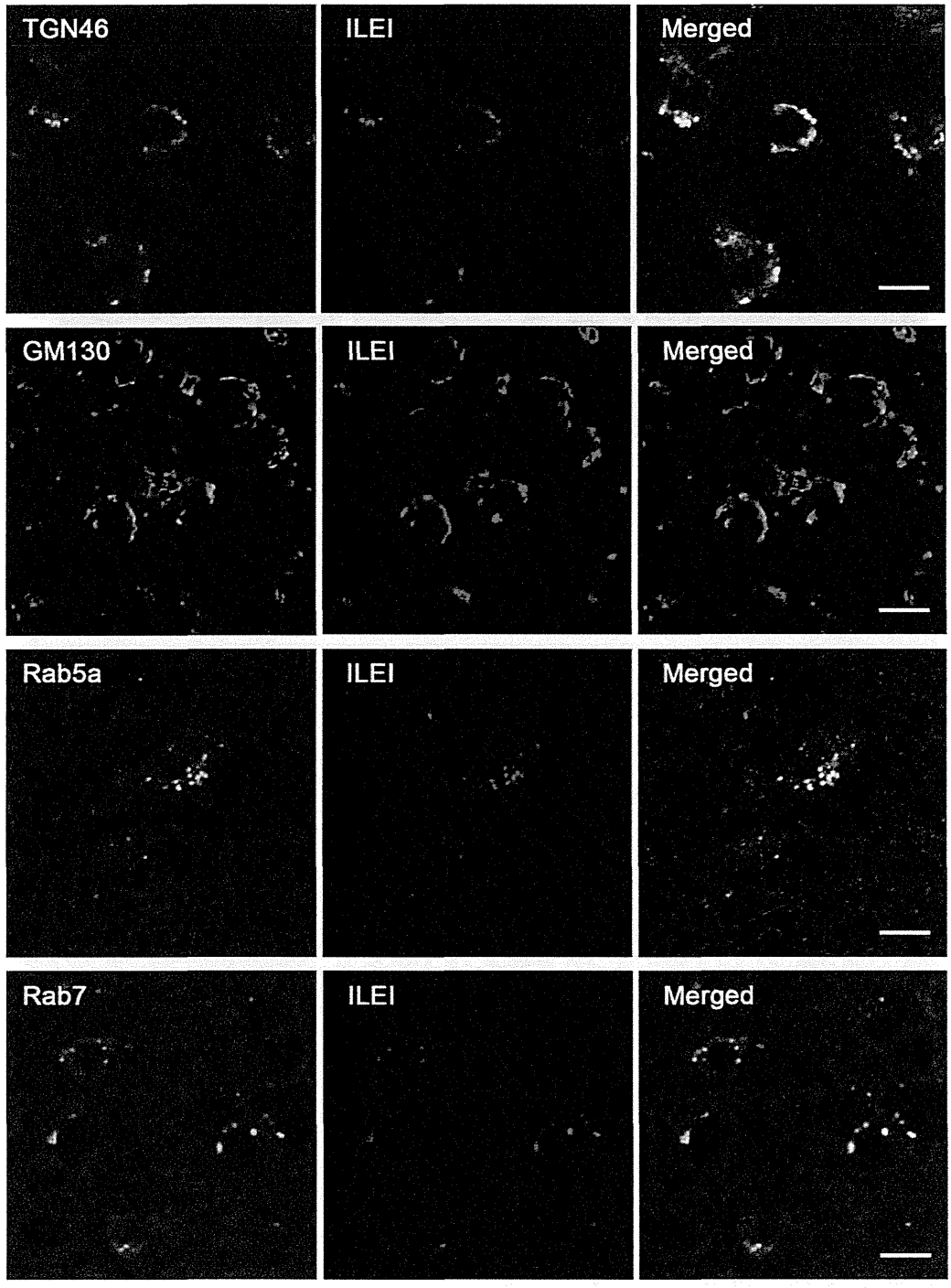

Supplementary Figure 7. ILEI is localized in the *trans*-Golgi network (TGN) and endosomes

Double immunostaining of mouse brain for ILEI and markers of the Golgi complex and endosome compartments. Antibodies against TGN46 (1:4,000, Sigma), GM130 (1:2,000, BD Transduction Laboratories), Rab5a (1:500), and Rab7 (1:300) (Santa Cruz Biotechnology) were used as markers of the TGN, *cis*-Golgi, early endosomes, and late endosomes, respectively. Scale bars: 20 μm.

Supplementary Figure 8

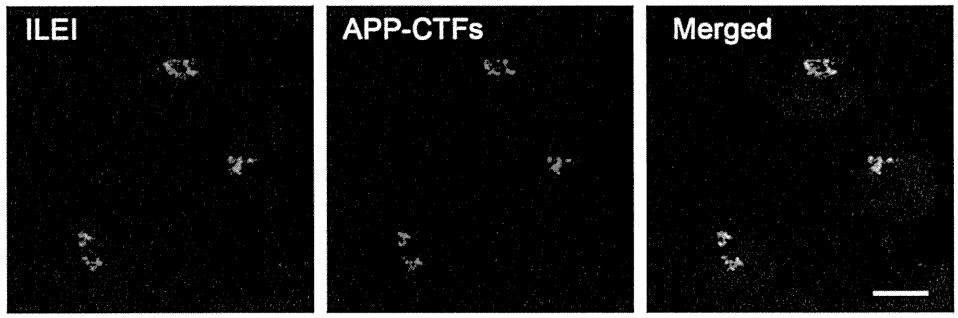

Supplementary Figure 8. Colocalization of ILEI and APP-CTFs

Double immunostaining for ILEI and APP-CTFs. HEK293 cells were stained with anti-ILEI antibody (1:4,000) and anti-APP-CTF antibody (1:3,000, Sigma). Nuclei were stained with Hoechst 33342. Scale bar: 10 μm.

Supplementary Figure 9

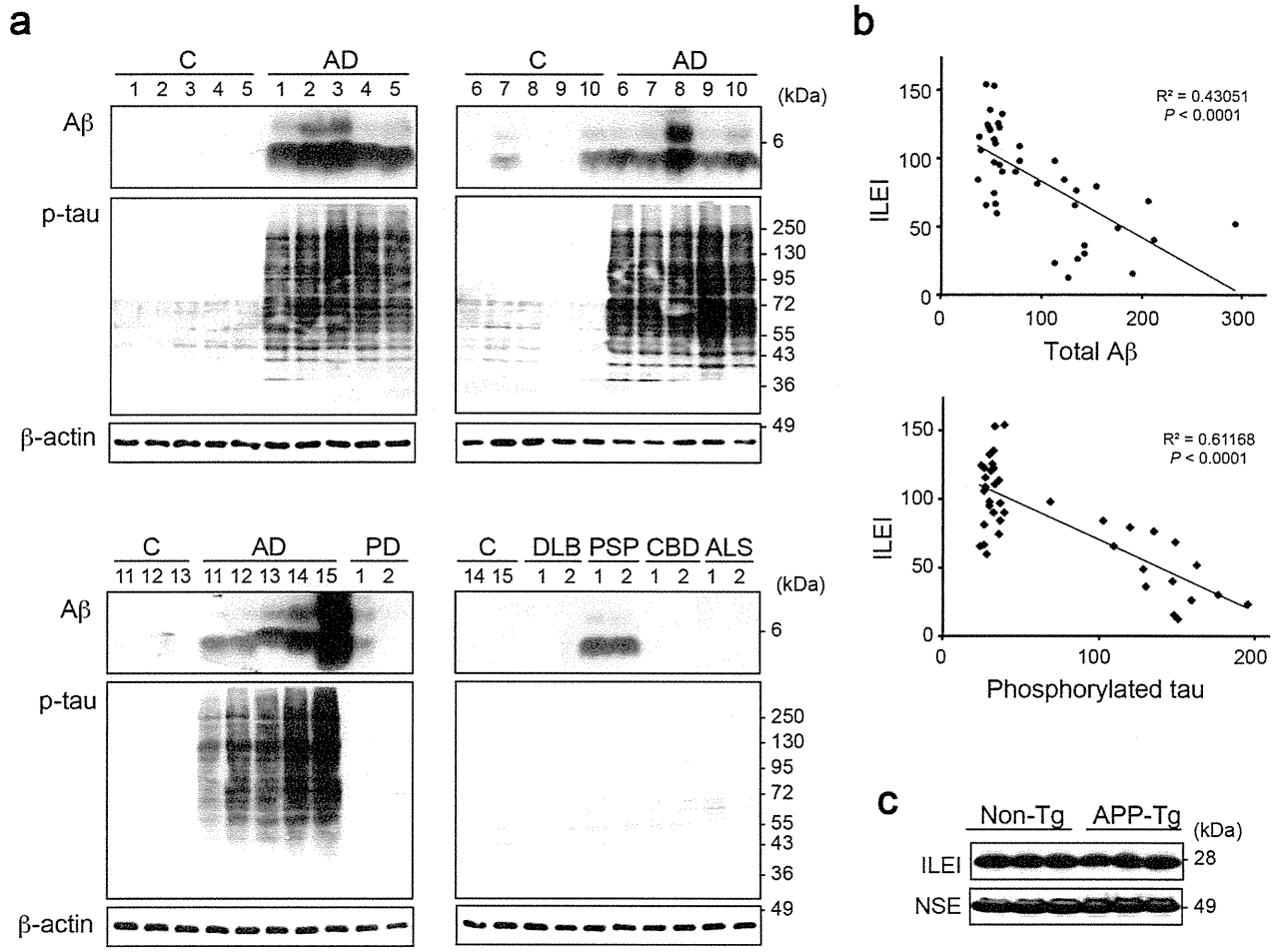

Supplementary Figure 9. Phosphorylated tau, Aβ, and ILEI in autopsy brains and ILEI level in APP-Tg mouse brains

(a) Lysates of temporal cortices of autopsy cases were subjected to immunoblotting for total Aβ and phosphorylated tau (p-tau). Blots were probed with anti-Aβ antibody (1:1,000, 4G8 from Covance) or anti-phosphorylated tau antibody (1:3,000, PHF13 from Millipore). β-actin was used as a loading control. C: control, AD: Alzheimer's disease, PD: Parkinson's disease, DLB: dementia with Lewy bodies, PSP: progressive supranuclear palsy, CBD: corticobasal degeneration, ALS: amyotrophic lateral sclerosis. **(b)** The graphs show the correlation between ILEI (see Fig. 5c) and Aβ or phosphorylated tau. The intensities of total Aβ and phosphorylated tau were measured with Image-J software and normalized to the intensity of β-actin. Linear regressions were performed using a Prism 3.0 software (GraphPad, San Diego, CA, USA). **(c)** Brain lysates from APP-Tg and non-Tg littermate mice (12 months old, $n = 3$ per genotype) were subjected to immunoblotting for ILEI. NSE was used as a loading control. Original immunoblots for (**a**) and (**c**) can be found in Supplementary Fig. 10.

Supplementary Figure 10

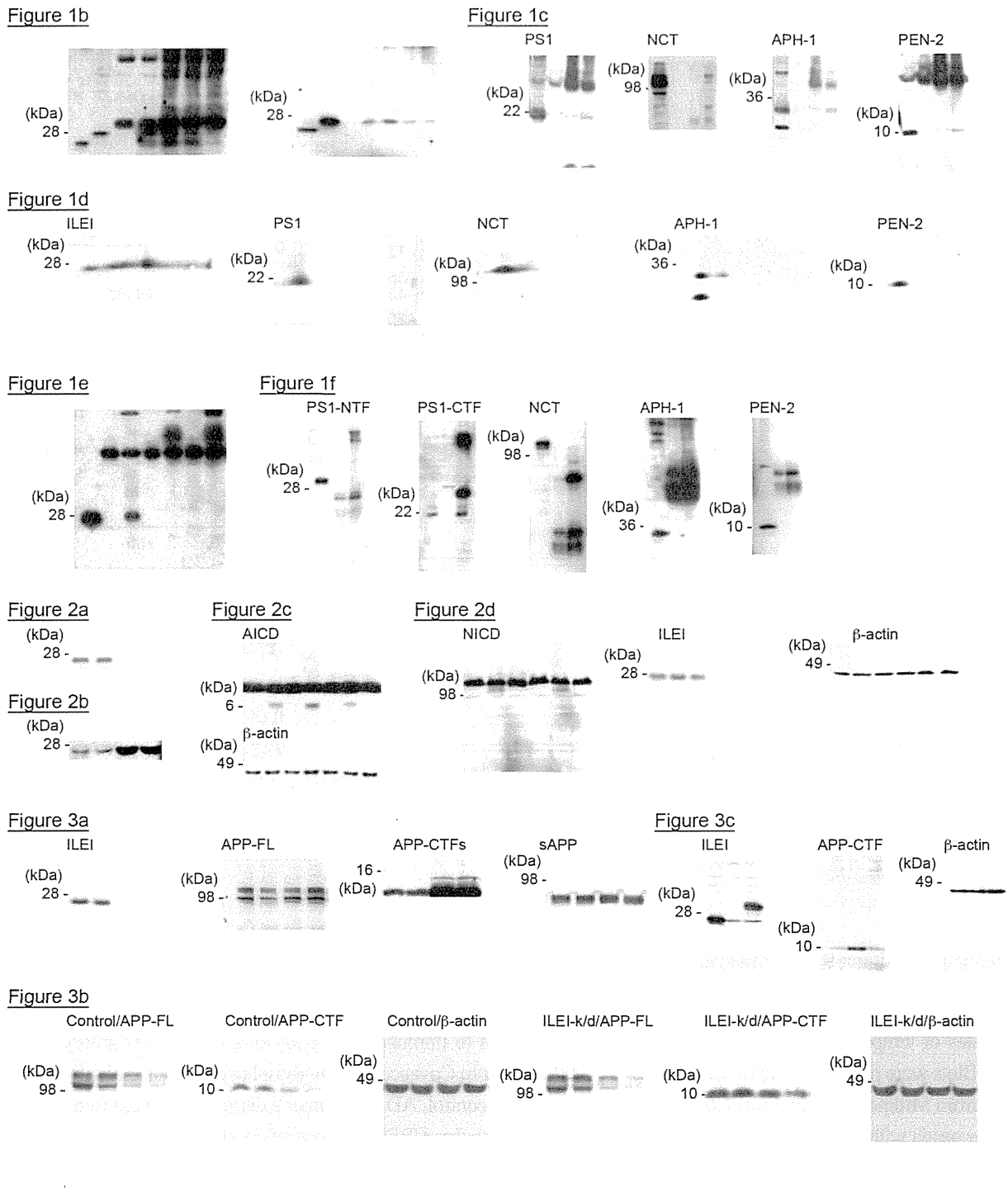

Supplementary Figure 10. Original immunoblots in main and supplementary figures.

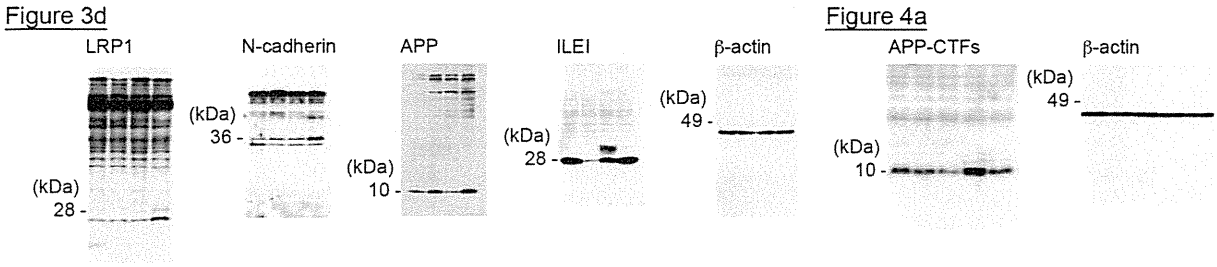

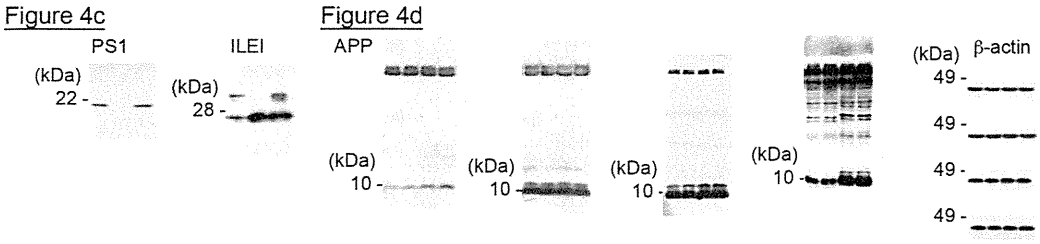

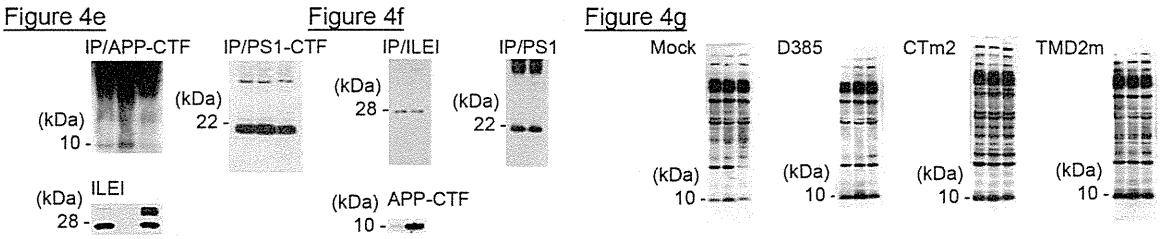

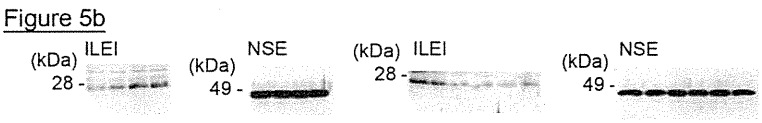

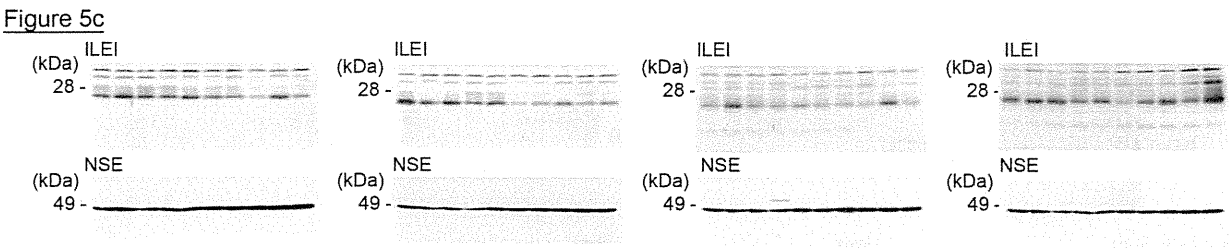

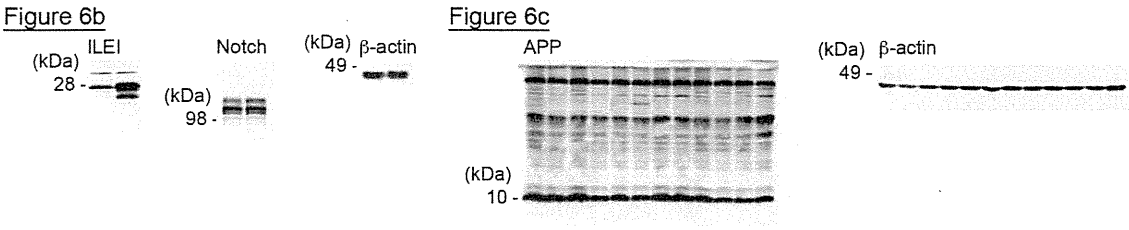

Supplementary Figure 10 continued.

Supplementary Figure 1a

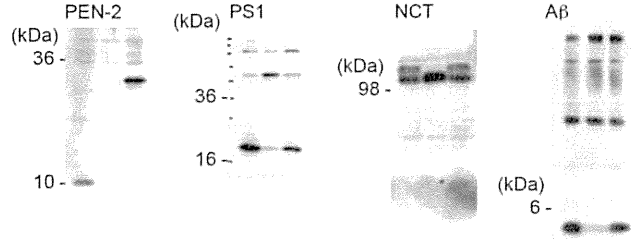

Supplementary Figure 1b

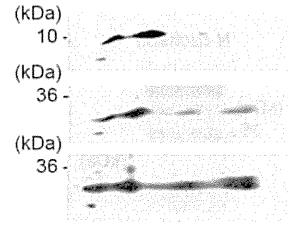

Supplementary Figure 2a

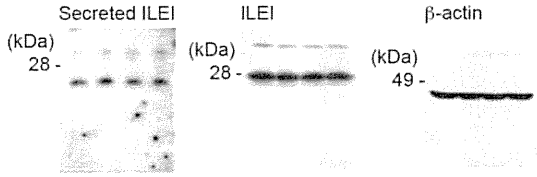

Supplementary Figure 2b

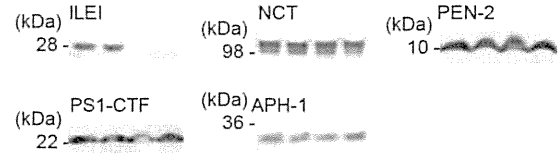

Supplementary Figure 2c

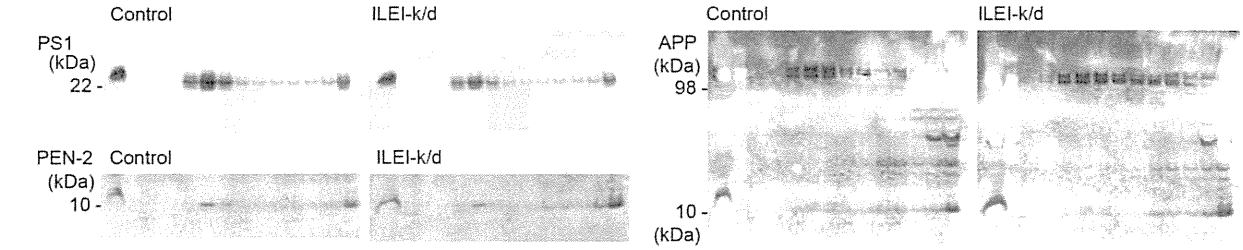

Supplementary Figure 3a

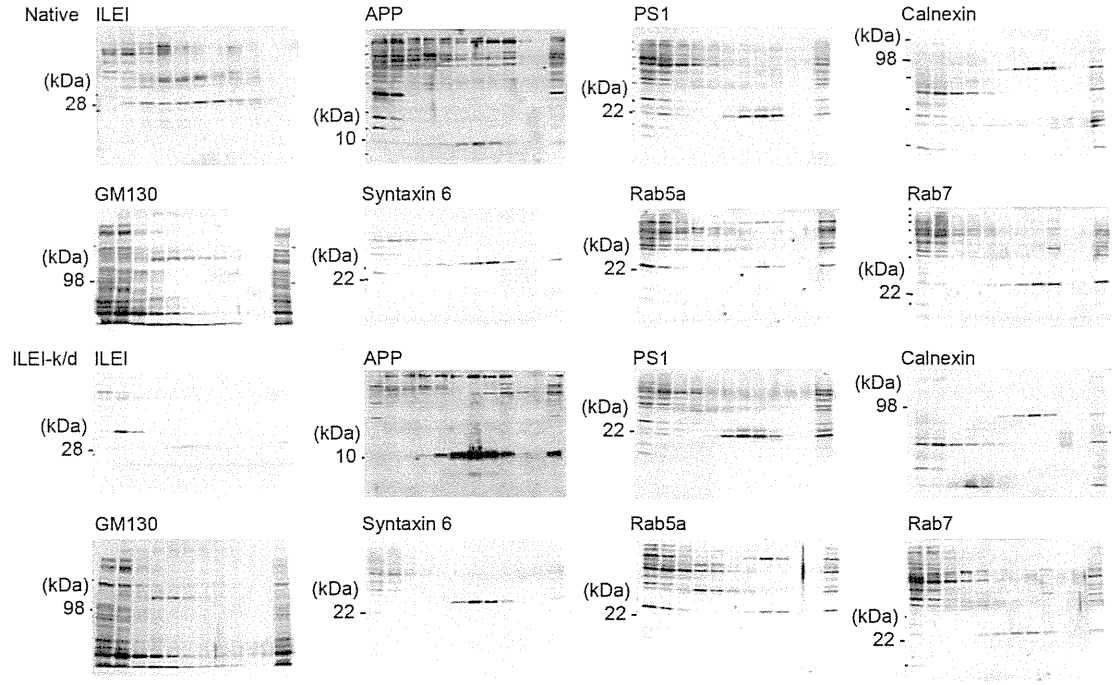

Supplementary Figure 10 continued.

Supplementary Figure 3a

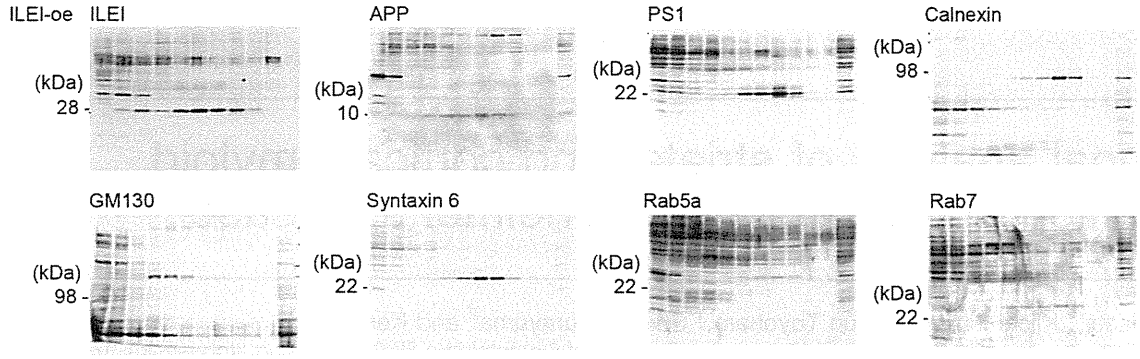

Supplementary Figure 3c

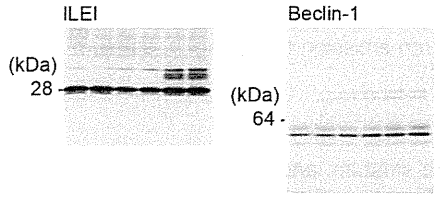

Supplementary Figure 3d

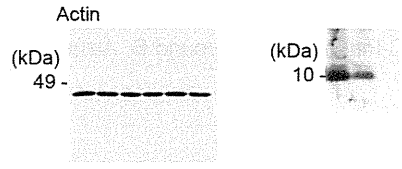

Supplementary Figure 4a/b

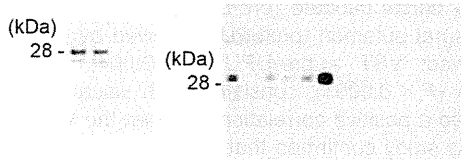

Supplementary Figure 5b

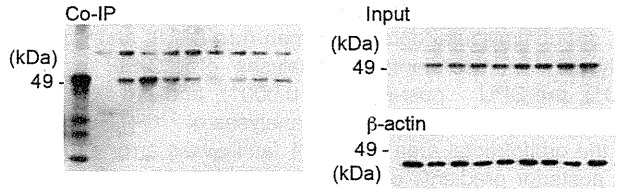

Supplementary Figure 5c

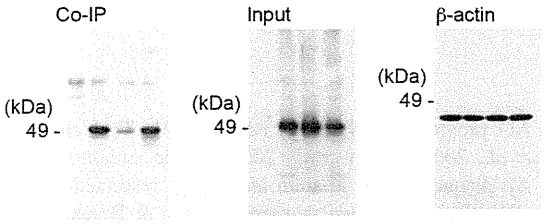

Supplementary Figure 5d

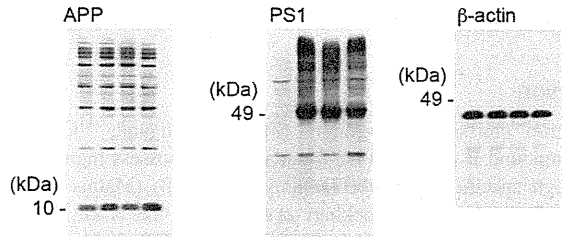

Supplementary Figure 9a

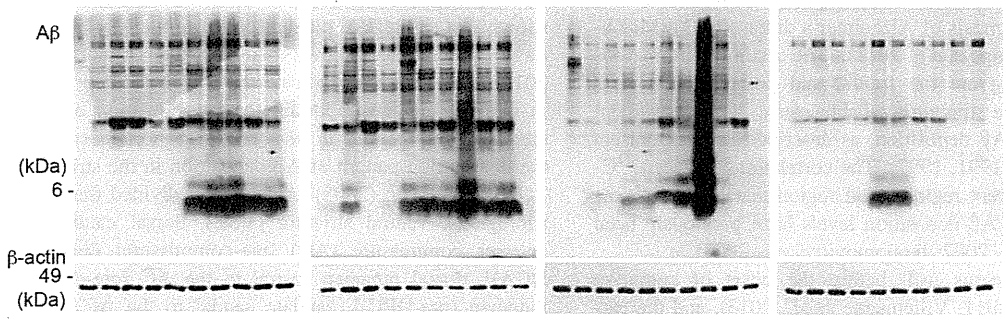

Supplementary Figure 9c

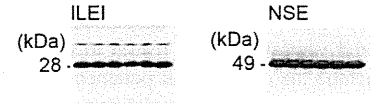

Supplementary Figure 10 continued.